Hindawi
Journal of Spectroscopy
Volume 2022, Article ID 3887038, 25 pages
https://doi.org/10.1155/2022/3887038

Review Article

Laser-Induced Breakdown Spectroscopy (LIBS) for Trace Element Detection: A Review

Z. H. Khan,[1] **M. Hedayet Ullah**,[2] **Bulu Rahman**,[3] **Aminul I. Talukder**,[1] **Md. Wahadoszamen**,[1] **K. M. Abedin**,[4] **and A. F. M. Y. Haider**[1,5]

[1]*Department of Physics, University of Dhaka, Dhaka 1000, Bangladesh*
[2]*Department of Physics, Bangladesh University of Textiles (BUTEX), Dhaka 1208, Bangladesh*
[3]*Department of Physics, Bangabandhu Sheikh Mujibur Rahman Science and Technology University, Gopalganj, Bangladesh*
[4]*Department of Physics, College of Science, Sultan Qaboos University, Muscat 123, Oman*
[5]*Department of Mathematics and Natural Sciences, BRAC University, Dhaka 1212, Bangladesh*

Correspondence should be addressed to Z. H. Khan; zulfiqarshuvo@du.ac.bd

Received 13 February 2022; Accepted 30 April 2022; Published 21 May 2022

Academic Editor: Nives Galić

Laser-induced breakdown spectroscopy (LIBS) has emerged as a promising technique for both quantitative and qualitative analysis of elements in a wide variety of samples. However, conventional LIBS suffers from a high limit of detection (LoD) compared with other analytical techniques. This review briefly discusses several methods that demonstrate the applicability and prospects for trace element detection while lowering the LoD when coupled with LIBS. This review compares the enhancement mechanisms, advantages, and limitations of these techniques. Finally, the recent development and application of LIBS coupled techniques for trace element detection are also discussed for various samples such as metal alloys, biomaterials, rare earth elements, explosives, drinking water, and water bodies.

1. Introduction

Any element with an average concentration below 100 parts per million (<100 ppm) or less than 100 micrograms per gram (<100 μg/gm) is considered a trace element. Trace elements, even present in small concentrations, can be either beneficial or hazardous, and they can considerably modify materials' characteristics. For example, heavy metals, such as arsenic and cadmium, can have an adverse effect on health even at trace levels. On the other hand, trace elements play a significant role in vital steel properties such as strength, corrosion resistance, hardness, and toughness. Therefore, reliable and robust detection of elements at a trace level is critical in various scientific, industrial, and technological sectors.

Laser-induced breakdown spectroscopy (LIBS) is a novel atomic emission spectroscopic technique for analyzing materials. LIBS uses a high-power pulsed laser to ablate a tiny part of the sample under investigation to generate a weakly ionized plasma on the surface. As this plasma expands and subsequently cools, the characteristic atomic/ionic spectral lines (popularly referred to as LIBS spectral lines) are emitted by the excited atomic/ionic species present in the microplasma. Since the optical emission from the microplasma contains the spectral signature of all the elements present in the sample material, one can quickly determine the elemental composition of the sample under study by analyzing its LIBS spectra. LIBS has the exceptional ability to perform a multielemental real-time analysis, which is not possible by any other conventional methods [1–5]. However, due to its relatively modest sensitivity, trace element detection by LIBS is still challenging, which is considered a significant limitation of this technique.

To date, several studies have been conducted to improve the sensitivity of the LIBS technique by including either additional experimental techniques or analytical approaches. The first part of this comprehensive review focuses on a detailed discussion of various techniques coupled with

LIBS that enable trace element detection at the ppm level or lower. One of the most frequent approaches for increasing the sensitivity of LIBS is utilizing a double-pulse laser. Another popular enhancing strategy is to employ an additional energy source/tunable laser to enhance the plasma to lower the detection limit of a trace element. Examples of this enhancing strategy are: LIBS coupled with laser-induced fluorescence (LIBS-LIF) [6], spark-discharge-assisted laser-induced breakdown spectroscopy (SD-LIBS), LIBS coupled with magnetic/electric field, and surface-enhanced LIBS (SENLIBS). Another effective technique to boost the signal and lower the LoD is combining LIBS with liquid-to-solid phase conversion (LIBS-PT). Examples of LIBS-PT are adsorption coupled LIBS, SENLIBS, and NELIBS, where nanoparticles (NP) and analyte solutions are dried on a substrate [7]. Lastly, LIBS coupled with multivariate analysis is necessary to discriminate compounds such as explosives, alloys, and biomaterials from other materials where identification of multiple trace elements is essential.

In this review, we present different variants of LIBS that were proposed to overcome the challenge faced for trace element detection, with basic principles and succinct descriptions, along with their compelling advantages and inevitable disadvantages.

The second part of the review elaborates on the applications and recent developments of these LIBS coupled approaches in different fields. These techniques have become a prominent analytical approach for the real-time monitoring of metallurgical products and metal alloys. Moreover, these techniques have excellent potential to analyze micronutrients and heavy metals in food and plants and detect rare earth elements (REEs) in geological minerals or ores. In addition, LIBS-PT has been found to have a great potential for monitoring toxic elements such as heavy metals in freshwater and wastewater, which is indispensable to help prevent direct or indirect exposure to these toxic trace elements. Furthermore, LoDs achieved under various experimental conditions in different fields have also been compiled in this review.

2. Different Types of LIBS Systems for Trace Element Detection

Several approaches for enhancing LIBS sensitivity and lowering LoDs have been proposed for trace element detection having an average concentration at parts per million (ppm) or sub-ppm level. These approaches have given unique features to the LIBS technique either by adding a second energy source to traditional LIBS or combining LIBS with other techniques.

2.1. Single-Pulse LIBS. Figure 1 depicts a typical schematic diagram of the experimental setup for single-pulse LIBS. The excitation laser is a Q-switched Nd:YAG laser with a pulse duration of 8 ns, a repetition rate of 10 Hz, and maximum pulse energy of 850 mJ, and an output at the fundamental wavelength of 1064 nm [8, 9]. A harmonic generator employing KDP crystal can generate up to fourth harmonics of the fundamental [10, 11]. The development of sensitive optical detectors such as intensified CCD (ICCD) has tremendously improved LIBS's ability to determine trace elements. After a software-controlled adjustable time delay, the Nd:YAG laser pulse electrically triggers the intensified CCD (ICCD) camera [12, 13]. This strategy greatly diminishes the strong background formed by the high-temperature plasma and hence offers the LIBS technique to detect atomic/ionic emission lines of trace elements with ease and precession [14].

2.2. Modification of LIBS System for Sensitive Trace Element Detection

2.2.1. Double-Pulse LIBS (DP-LIBS). Double-pulse LIBS (DP-LIBS) employs two laser pulses from two different laser sources or from the same source to ablate the sample, resulting in enhanced atomic emission intensity and thereby lower LoDs [16, 17].

In collinear double-pulse mode (Figure 2(a)), the first pulse ablates the sample; plasma is induced; and then the second pulse will reheat the plasma, or a portion will be used to create another plasma. Plasma production, plasma temperature, and electron density can be maximized by choosing a suitable interpulse delay resulting in enhanced atomic emission [18–20]. Other possible geometrical configurations include orthogonal preablation, orthogonal reheating, and dual pulse crossed beam modes used in DP LIBS to increase the intensities of atomic emission lines [21].

Two angled laser beams overlap at the sample surface in the crossed beam configuration (Figure 2(b)) [22]. In orthogonal reheating DP LIBS configuration (Figure 2(c)), plasma is produced by the first laser pulse propagating orthogonal to the target surface, whereas the resulting plasma is reheated by a successive delayed pulse focused parallel to the target surface [23]. In orthogonal preablation configuration (Figure 2(d)), the first laser pulse is focused parallel to and at some distance above the sample surface, resulting in the formation of air plasma [24]. Then a delayed second laser pulse, orthogonal to the first pulse, is focused on the target surface at normal incidence for ablation [25].

2.2.2. Femtosecond LIBS (fs-LIBS). After the chirped pulse amplification technique (CPA) was developed, the promise of ultrashort pulses for LIBS analysis has increased manifolds. Typically, a mode-locked Ti:sapphire laser is employed as an fs laser source (Figure 3).

Because of the ultrashort duration of the fs pulse, it deposits all the energy onto the target surface without interacting with the resulting plasma [27], which contrasts with ns laser ablation [28]. Unlike ns laser ablation, fs laser pulses are too short for producing ionization, sample heating, and vaporization until the ending of the laser pulse. The fs laser pulses are much shorter than the heat conduction time of electron and energy transfer time from electron to ion, both of which are in the picosecond range. Therefore, femtosecond LIBS offers significantly reduced heat-affected region and thermal damage due to insignificant

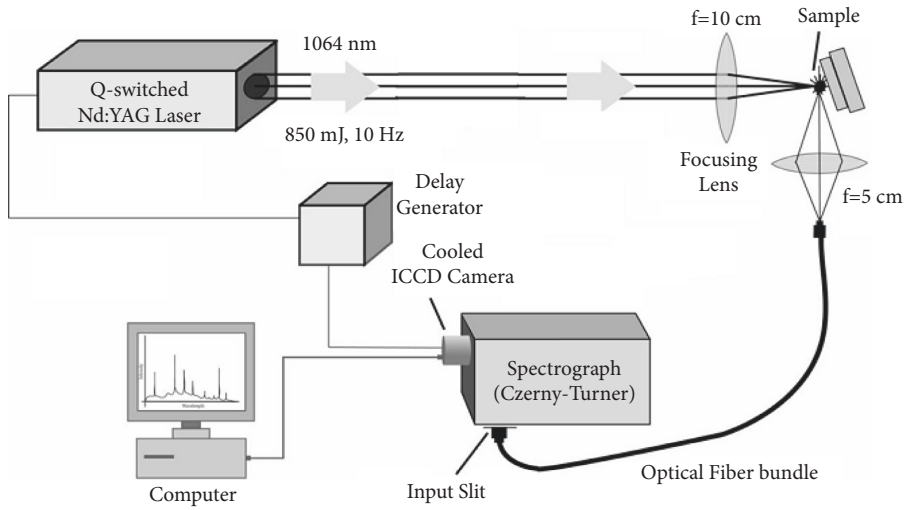

Figure 1: Schematic diagram of the LIBS experimental setup (adapted from [15]).

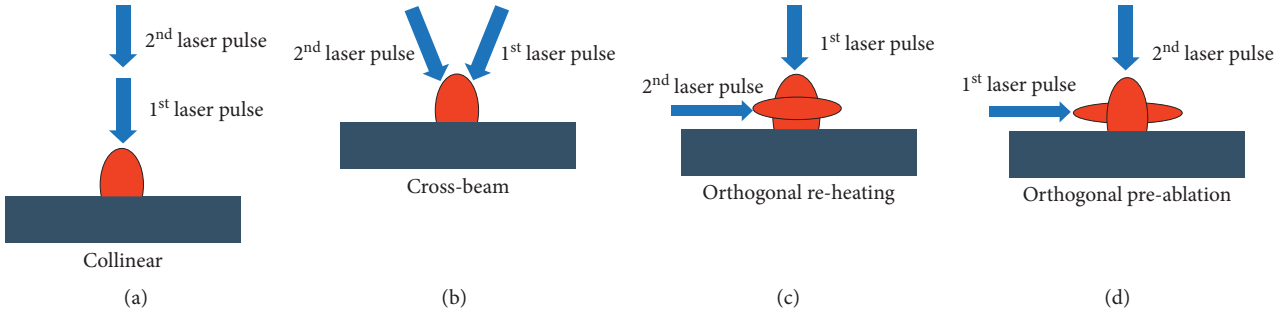

Figure 2: Four different DP LIBS configurations: (a) collinear, (b) cross-beam, (c) orthogonal reheating, and (d) orthogonal preablation (redrawn from [20]).

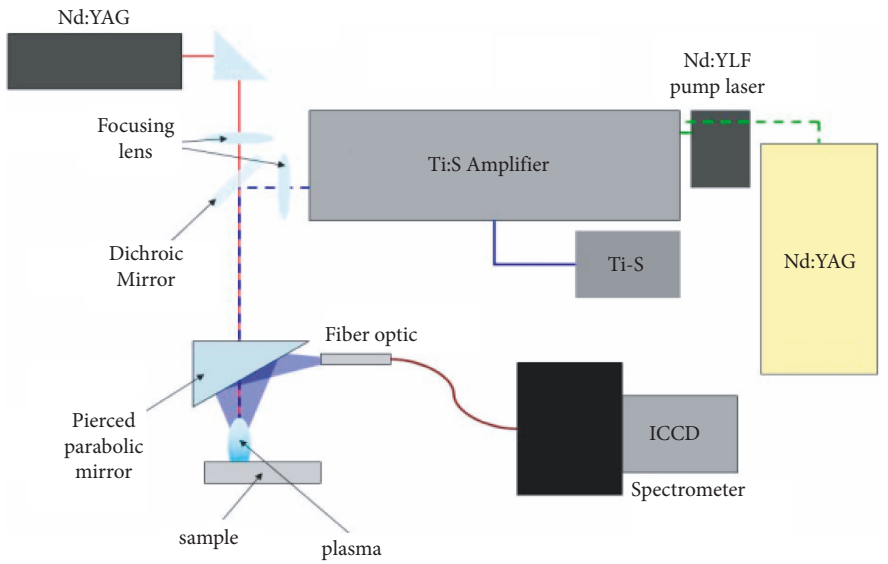

Figure 3: Schematic of the experimental setup of a femtosecond LIBS (adapted from [26]).

hydrodynamic motion and heat conduction throughout the laser pulse [29]. As a consequence, controlled material modification and removal are possible [27]. Other advantages of fs-LIBS over ns LIBS include higher spatial resolution, decreased continuum emission, and reduced plasma mixing from the atmosphere [30]. Employing filaments produced by UV femtosecond laser radiation enables beam propagation over long distances (5–100 m) [31] and has potential for remote LIBS helping rapid elemental analysis of distant targets [32]. On the other hand, the disadvantages of fs-LIBS are the much higher complexity of the fs laser system and significantly higher cost.

2.3. LIBS Coupled with an Additional Energy Source

2.3.1. LIBS Coupled with Laser-Induced Fluorescence (LIBS-LIF). The LIBS-LIF approach, first proposed by Measures and Kwong, utilizes two lasers. The first laser forms plasma, and the second laser re-excites atoms of the element of interest and eventually induces fluorescence emission from the atoms [33]. The hyphenated LIBS-LIF approach preserves the advantages of LIBS, such as online applications, while offering a much lower LoD, well below the ppm range. The LoD can be minimized by optimizing the ablation and excitation laser pulses' flux density and optimizing the delay between them [6].

2.3.2. Magnetic-/Electric-Field-Assisted LIBS. The high-intensity magnetic fields help enhance the emission from laser-induced breakdown plasma [34, 35]. Therefore, the energy imparted to the plasma can be well utilized by applying the magnetic field as it influences ionization and the lifetime of plasma and limits plasma expansion [35]. A homogeneous electric field also enhances the intensities of the atomic/ionic emission line and the S/N ratio. Therefore, highly congested emission lines can be identified easily [36, 37].

2.3.3. Spark-Discharge-Assisted LIBS (SD-LIBS). In spark-discharge-assisted LIBS (SD-LIBS), the strong electric field of the electrical spark causes an electron avalanche, which causes the plasma plume to expand inside an electrode pair [21]. SD-LIBS demonstrates significant enhancement in line intensities as well as considerable improvement of signal-to-noise (S/N) ratios [38] because SD-LIBS increases the electron density of the plasma instantly after the initial ablation of sample material [39].

2.3.4. Microwave-Assisted LIBS (MA-LIBS). In this technique, the microwave produced from an adjacent microwave cavity is resonantly coupled to the plasma (Figure 4). As a result, unbound electrons are excited, resulting in "hot electrons" that eventually excite more atoms and ions by collision [40]. Hence, plasma lifetime increases (from μs to ms), resulting in enhanced sensitivity [41]. However, remote interrogation of a target becomes complicated as the cavity-generated microwaves must be transmitted over short distances by antennas or waveguides.

2.3.5. Resonance-Enhanced LIBS (RELIBS). Resonance-enhanced LIBS (RELIBS) is a variant of the two-pulse scheme in which plasma is generated and heated by photo-resonant excitation of the host species in the plume. The excitation wavelength is set to a strong absorption line of one of the main species by an optical parametric oscillator (OPO) laser. Through multistep collision, energy is transferred to the analyte [43]. When the fluence of the initial laser pulse is near the ablation threshold, the LoD improves by the most significant amount compared to ordinary LIBS [44]. RELIBS is exceptionally well suited for minimally destructive analyses. RELIBS has an advantage over LIBS-LIF because it can determine many species simultaneously [45].

2.4. LIBS Coupled with Other Techniques

2.4.1. LIBS-Raman. In a hyphenated LIBS-Raman system, the same laser is used for LIBS and Raman spectroscopy in sequence in a single set-up, simultaneously providing information about the material's elemental composition and molecular composition [46]. Unlike typical CzernyTurner-based spectrographs, the ICCD is coupled with a broad band-pass (250–900 nm) echelle spectrograph with no moving dispersive elements. In addition, the echelle spectrograph provides high resolution with a fixed and very narrow width ($\sim 10 \times 50\,\mu$m) of the slit [46]. The LIBS-Raman approach can be a useful tool for sorting and identification of plastics [47], classification of inks and pigments [48], space exploration [49], analysis of kidney stones [50], and mineralogical and environmental applications [51].

2.4.2. Nanoparticle-Enhanced LIBS (NELIBS). NELIBS is based on the deposition of metallic NPs with a suitable interparticle distance on the solid (metal alloy and transparent samples) surface or nanoparticle-aqueous solutions (biological fluids and water) dried on a substrate. The interaction with the laser induces the oscillation of conduction electrons coherently and collectively in the metallic NPs. Resonance, termed localized surface plasmon resonance, occurs when the laser's frequency coincides with the plasma frequency of free electrons in the NPs [52]. In the gap between the NPs and near the particle surface, an order of magnitude increase in the incident laser's local electric field is observed [53]. This phenomenon can induce a faster breakdown than thermal vaporization as electron extraction from conductive material is much easier in this case [54]. The field enhancement depends on laser power and the concentration of NPs on the substrate's surface [55].

NELIBS has been advantageous, particularly for studying transparent samples such as glasses and gems. Therefore, laser-sample interaction can be avoided; the NPs absorb the laser energy to initiate the breakdown quickly. NELIBS

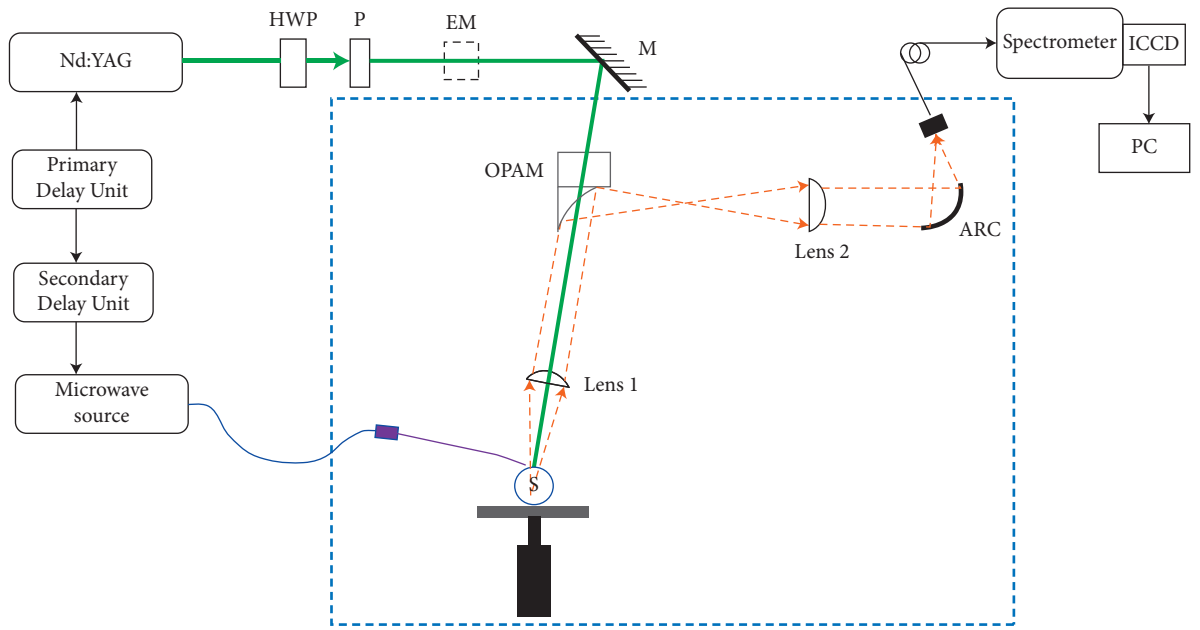

Figure 4: Schematic of the experimental setup of microwave-assisted LIBS (adapted from [42]).

technique can perform single-shot elemental analysis with LoD below the ppb level [56].

2.4.3. LIBS Coupled with Mathematical Methods. The analytic capabilities of LIBS can be significantly improved with proper spectrum analysis, and based on the spectrum's characteristics, appropriate mathematical methods should be chosen. Mathematical processing, such as the univariate methods, includes single linear regression [57], internal [58], or external standard [59]. The univariate analysis method establishes a correlation between the spectrum's intensity and the element's content. However, due to the spectral line's self-priming and self-etching effect and interference from other peaks, the fitting with a single variable suffers from poor prediction ability. In contrast, mathematical processing such as multivariate methods is found to be superior to univariate analysis. Multivariate analysis can fully utilize the spectrum to reduce matrix interference, remove redundant information, and extract relevant information in order to develop a quantitative model for improving the sensitivity and prediction ability [60]. Partial least squares (PLS) is the most frequent multivariate analysis (chemometric method) used by LIBS for concentration measurement [61]. Some other examples of multivariate methods include principal component analysis (PCA), artificial neural network (ANN) [62], random forest [63], vector machines regression model [64], multiple linear regression (MLR) [65], soft independent modeling of class analogy (SIMCA), and least absolute shrinkage and selection operator (LASSO) [66].

2.5. LIBS Coupled with Liquid-to-Solid Phase Transformation (LIBS-PT). In general, liquid-to-solid phase conversion is an effective technique for lowering the LoD. Examples of LIBS in combination with phase transformation (LIBS-PT) are SENLIBS, adsorption-coupled LIBS, NELIBS [7] (where NPs and aqueous samples are dried on the substrate), dispersive liquid-liquid microextraction LIBS [67], electrodeposition of heavy metal on an electrode [68], and metal precipitation followed by membrane separation [69].

2.5.1. LIBS Coupled with Adsorbate. Direct detection of dissolved trace elements by LIBS with adequate sensitivity is challenging in an aqueous solution. Detection sensitivity can be increased, and LoD can be lowered significantly if trace elements are adsorbed by a suitable adsorbent and then implementing LIBS on the composite solid matrix of trace element and adsorbent [15]. Examples of adsorbate used for liquid-to-solid conversion of samples are wood slice [70], bamboo charcoal [71], carbon planchet [72], ZnO [15], zeolite [73], porous electrospun ultrafine fibre [74], 3D nanochannel porous membrane [74], metallic substrate [75], and calcium hydroxide pellet [76]. The calibration curves usually have an initial linear part, and however, it subsequently demonstrates saturation, which suggests these curves to be Langmuir type isotherms [15, 73] (Figure 5). This characteristic saturation limits the highest concentration detected by adsorbent-coupled LIBS measurement of trace elements in liquid for a particular adsorption time and particular adsorbent [15, 73].

2.5.2. Surface-Enhanced LIBS (SENLIBS). In the case of surface-enhanced LIBS (SENLIBS), a microdroplet of liquid is smeared and dried on the surface of metallic substrates. The use of a metallic substrate aids in the signal enhancing process, as the plasma comprises a combination of species from the metallic substrate and the sample [77]. In SENLIBS, a low boiling point substrate provides higher detection

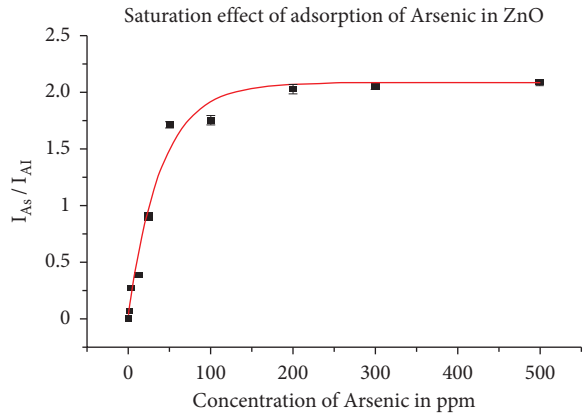

FIGURE 5: Saturation effect of calibration curve for adsorption of arsenic in zinc oxide adsorbent (adapted from [8]).

sensitivity [78]. SENLIBS is an effective enhancement technique that has been successfully used in the investigation of oil [79] and heavy metal elements in liquids [80, 81] with improved LOD and reduction of the matrix effect.

In chemical replacement SENLIBS (CR-SENLIBS), the inert and trace heavy metal ions are replaced rapidly by highly chemically active metal ions in the aqueous solution [80]. For example, Pb, Cr, Cd, and Cu in an aqueous solution can be replaced sufficiently by Mg on the magnesium alloy within only 1 min. After that, the concentration of each heavy metal can be found by SENLIBS on a magnesium alloy surface [80].

3. Comparative Study of Different LIBS Systems

Table 1 briefly summarizes the advantages, disadvantages, and key features of different types of LIBS systems discussed in Section 2.

4. Applications of LIBS for Trace Elements Detection

4.1. Analysis of Metals and Metal Alloys. Metal alloy properties, such as strength, corrosion resistance, hardness, and toughness, depend mainly on the minor and trace elements [87–89]. Several approaches have been proposed to improve the analytical sensitivity of LIBS; DP-LIBS (Section 2.2.1) is one of them. Jiang et al. [90] explored the combined effect of several ambient environments in terms of gas and pressure with DP-LIBS to enhance the detection sensitivity of the technique. They found that the LoDs of C and S in steel obtained with double-pulse excitation in a vacuum were approximately three times better than those obtained with single-pulse excitation. Cui et al. [91, 92] employed a long-short DP-LIBS to determine Mn and C in the steel. Using this method, the linearity fit (R^2) was improved up to 0.988 and 0.9667 for Mn and C, respectively.

The analytical benefits of using double-pulse excitation in the LIBS system to determine minor elements in aluminum alloys were evaluated by Ismail et al. [93]. Spectral lines of Mg, Ti, Cr, Mn, Fe, Ni, and Cu were selected to build the calibrations curves where the Voigt function was used for fitting. Under optimum conditions, DP-LIBS provided significantly improved LoDs within 4–100 ppm for all the examined elements in aluminum. Sun et al. [94] employed spatially resolved double-pulse excitation in the LIBS experiment for the multielement detection of aluminum alloys. Calibration curves of Fe, Cu, Mg, Mn, Zn, Sn, Pb, Ni, Ti, Cr, Ca, and Sr were obtained at six different positions (0.36 to 2.16 nm) of the plasma plume, and the lowest LoDs for each element were found at the center of the plasma (1.08 nm) in DP-LIBS. The LoDs of all the elements of interest were achieved in the range of 0.56 to 27.41 ppm. Hai et al. [95] proposed a 10 μs delay between annular and circular nanosecond laser pulse in DP-LIBS for enhancing signal intensity and reducing LoDs of trace elements Li and Mg in aluminum alloy. In comparison with SP-LIBS (Section 2.1), the proposed DP-LIBS method observed about four times signal augmentation and three times LoD reduction (Figure 6).

Santagata et al. [96] used the femtosecond DP-LIBS technique to trace Pb, Sn, and Zn in copper-based alloys. The emission intensities of the investigated trace elements were normalized with a Cu (I) emission line, and a linear regression coefficient within the range of 0.996 to 0.999 was observed.

Abbasi et al. [97] applied MF-LIBS (Section 2.3.2) to enhance the signal intensity of palladium (Pd) plasma. For MF-LIBS, a 3–4-fold enhancement of optical emission intensity was observed for Pd-I and Pd-II lines compared to LIBS only (Figure 7). It was noticed that the effect of the magnetic field on signal enhancement is element-dependent. Hao et al. [98] introduced LIBS assisted with ring-magnet confinement to improve the detection sensitivity of trace vanadium (V) and manganese (Mn) in steel. In this technique, an external magnetic field influenced the movement of electrons and ions in the plasma plume to increase plasma temperature and electron density. The LoDs of V and Mn in steel were decreased to 11 and 30 ppm by employing a ring magnet, respectively. Al Shuaili et al. [42] utilized MA-LIBS (Section 2.3.4) to detect palladium in solid samples, where 92-fold improvements in the signal intensity were noticed. The LoD for MA-LIBS was 5 ppm, which was found to be 8 times greater than the conventional LIBS.

Some spectral lines of interest such as P (178.3 nm) and S (180.7 nm) are in the vacuum UV range, and it is significantly challenging to detect these lines using an ordinary spectrometer operating in air. However, without using a vacuum chamber, the LoD of trace elements such as phosphorous in steel can still be improved if LIBS-LIF is employed (Section 2.3.1) [99]. The LoD of P in steel was 0.7 ppm, better than conventional LIBS [99]. Li et al. [100] introduced a wavelength-tunable optical parametric oscillator (OPO) laser and an Nd:YAG laser to selectively enhance boron spectral line intensities in nickel-based superalloys to improve the quantitative analysis of trace boron. B I 208.96 nm line intensity was enhanced up to 5.8 times with a 249.77 nm OPO laser. With this LIBS-LIF approach, the LoD of trace boron was 0.9 ppm. LIBS-LIF with a ground-state atom excitation (LIBS-LIFG) has a lower

Table 1: Comparative study of different types of LIBS techniques used for trace element detection.

Method	Key points	Advantage	Disadvantage
Single-pulse LIBS (SP-LIBS)	A single-laser pulse of short duration and high power initiates breakdown to produce laser plasma	Low cost, less complexity of the experimental setup	Suffers from low sensitivity and high LoD
Collinear DP-LIBS	Increased emission due to greater material ablation, enlarged plasma volume, and reheating of plasma produced from second pulse [82]	(i) The simplest method for implementing the DP [82] (ii) Enhanced emission signals and improved signal to background ratio compared to SP-LIBS (iii) Same laser and the same optical system be used to focus the two pulses [1] (iv) Only geometric configuration for standoff applications	Experimental setup becomes more complicated and costly than SP-LIBS
Orthogonal DP-LIBS	Involve a combination of effects, including increased plasma volume and temperature, increased laser/sample interactions, formation of a preionized region above the sample, and direct surface effects such as heating	(i) Provides higher signal enhancements than the collinear configuration for numerous samples (ii) A combination of nanosecond and femtosecond pulses can be used [2] (iii) In comparison to collinear DP-LIBS, it is easier to align [1] (iv) Provide maximum flexibility by allowing the pulse energies to be separately modified [1]	(i) Two sets of focusing optics are needed (ii) Two lasers are often needed
Femtosecond LIBS	The high-pulse peak power removes the material and transforms it into vapor or plasma phase without melting	(i) Improves the precision of LIBS measurements instead of sensitivity (ii) More reproducible threshold power at which ablation occurs (iii) Greatly reduce sample material redeposition	High cost and complexity of femtosecond laser compared to ns laser
Resonance-enhanced LIBS (RELIBS)	The second laser, unlike LIBS-LIF, is tuned to the wavelength of a strong absorption line of one of the primary species of the matrix atoms of the plasma, and through particle-particle collisions, the absorbed energy is distributed over all other elements [45]	(i) Unlike LIBS-LIF, multiple species can be determined simultaneously [45] (ii) Unlike conventional LIBS, a small amount of matter is ablated and, therefore, is minimally destructive [45]	Requirement of a tunable laser, such as an optical parametric oscillator (OPO)
Combining LIBS and Raman	Provide complementary information of a complex sample	(i) Useful for simultaneous atomic and molecular analyses by the same experimental setup [4] (ii) This hyphenated technique enables sensitive detection of nonmetals as like metal elements	(i) Limitation involved with echelle spectrometer, that is, low data acquisition rate and increased dead zones beyond 700 nm [4] (ii) For a strong emission line, a saturation of some pixels of the CCD occurs with an increased gate width of the intensifier [2]
Combining LIBS and LIF	A trace element in the plasma is resonantly exited by a second laser beam of a particular wavelength	LoDs down to ppb level is achievable	(i) Simultaneous multielement detection is not possible [2] (ii) Needs additional tunable lasers such as optical parametric oscillator (OPO) laser
LIBS with magnetic/electric field	Under the magnetic field, expansion of the plasma plume is slowed down because of Lorentz force results in an increase in plasma density, and electron-ion recombination rate increases, and emission-line intensity is enhanced [65]	Highly congested lines can be identified easily	(i) Inconvenient for in situ detection (ii) Needs an additional energy source

Table 1: Continued.

Method	Key points	Advantage	Disadvantage
Spark discharge assisted LIBS (SD-LIBS)	Signal enhances due to plasma reheating by the discharge, increased plasma size, and prolonged temporal evolution of emission from plasma	(i) Requirement of lesser laser pulse energy [38] (ii) Less sample surface damage [38] (iii) Gas transportation or a vacuum system is not required [38] (iv) Unlike DP-LIBS, an economic and easy-to-implement high-voltage discharge circuit is required	
Nanoparticle-enhanced LIBS (NELIBS)	Colloidal solution of nanoparticles (a few microdrops) are dropped on a small area of the sample	(i) Experimental setup modification is not needed (ii) Simple and inexpensive sample preparation (iii) Can be combined with other techniques such as femtosecond double-pulse [83] and magnetic field-assisted LIBS [84] (iv) Particularly advantageous for studying transparent samples such as glasses and gems	(i) It is important that the laser spot is focused inside the circle of the deposited NPs where their concentration is more homogeneous (ii) Colloidal solution of NP should be free from contamination and residual reactants that can interfere with the measured analyte
Surface-enhanced LIBS (SENLIBS)	Signal enhancement occurs from the plasma mixture obtained from the sample and metallic substrate	Even the inert and trace heavy metal ions (Cu, Pb, Cd, and Cr in an aqueous solution) can be sensitively detected by chemical replacement SENLIBS	(i) Primarily suitable for liquid sample (ii) The solid sample must be transformed into a liquid first and then dried on the substrate
Microwave-assisted LIBS	Microwave radiation is coupled to the regions of the plasma where the electron density is below the critical electron density [41]	(i) Offers an improved LoD at low laser energy (ii) The low laser energy significantly avoids sample damage [85]	(i) Complex experimental setup because of the requirement of microwave generators, waveguides, and near field applicators [85] (ii) Not suitable for standoff applications since the setup has a near-field applicator
LIBS coupled with mathematical methods	The univariate and multivariate chemometric methods can be combined with LIBS to improve the identification, classification, and quantification of trace elements	(i) Matrix interference can be minimized, and the spectrum can be completely utilized [86] (ii) Improves sensitivity and can obtain a quantitative model having good predictive ability [60] (iii) Dramatic improvement in discrimination/classification capability of LIBS (iv) Can filter out redundant information in the spectrum [86]	Mathematical methods must be carefully chosen; otherwise, it demonstrates poor analytical performance [86]
LIBS coupled with adsorbate	Trace elements are adsorbed by an adsorbent and then implementing LIBS on a solid matrix comprised trace elements and adsorbent	An effective and inexpensive method for lowering the LoD	The calibration curve demonstrates the characteristic saturation, which limits the highest concentration to be detected

LoD and higher analytical performance than LIBS-LIF with excited-state atom excitation (LIBS-LIFE; Figure 8).

Goueguel et al. [44] introduced RELIBS (Section 2.3.5) approach to investigate the signal-to-noise ratio of Mg I 285.21 nm line in aluminum alloys. They investigated the effect of four optimum parameters such as excitation wavelength, ablation fluences, excitation fluences, and interpulse delay on the SNR of Mg (285.21 nm). The LoDs of Mg and Si in aluminum were 21 and 1,438 ppm, respectively, using RELIBS under optimum conditions. In a subsequent study, the same group applied RELIBS and selective excitation of Al I 309.27 nm to enhance the detection sensitivity of trace Mg and Si in aluminum alloys [45]. In this method, the excitation energy of Al I 309.27 nm was transferred to all the components of the plasma plume, including the trace elements Mg and Si, through particle collisions. Using the optimum operating conditions, the LoDs were 0.75 and 80 ppm for Mg and Si, respectively, far better than the previous experiment. In another approach, Khedr et al. [102] spread gold nanoparticles on aluminum alloy, employed NELIBS, and observed approximately a two/three times improvement of the intensities of the aluminum

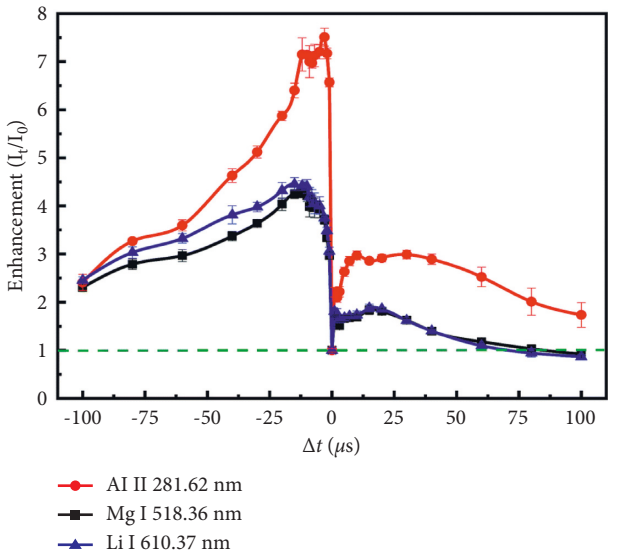

FIGURE 6: Signal enhancement for DP-LIBS as a function of interpulse separations, Δt [95].

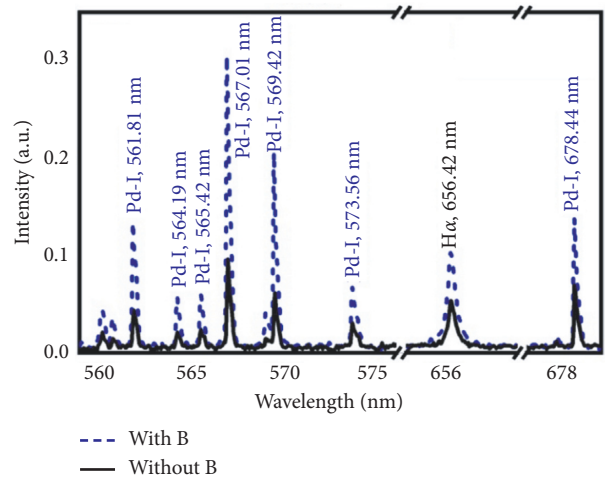

FIGURE 7: Optical emission spectrum of palladium for laser fluence of 12.6 J/cm^2 recorded before and after applying magnetic field [97].

atomic lines, whereas, in the case of atomic lines of Mg, about eight times signal enhancement is observed.

A high repetition rate SD-LIBS (Section 2.3.3) was developed by Jiang et al. [103] to improve the detection sensitivity of trace elements in copper. A 3–9-fold improvement of the LoDs of Pb, Fe, and Al under this experimental condition was achieved, and the LoDs were 240, 113, and 30 ppm, respectively. A similar technique with lock-in signal detection was employed by Kang et al. [104] to analyze Pb and Al in Brass, and LoDs were found to be 0.112 and 0.178 ppm, respectively.

LIBS coupled with a mathematical method (Section 2.4.3) was evaluated to quantify trace elements in steel [105–107]. Sarkar et al. [105] reported that with a precision of about 4–9%, the PLS model demonstrated remarkable success in identifying Mo and Co at the level of hundreds of ppm. The LoD of Cr and Ni was achieved with an accuracy of 2%. Sun et al. [106] demonstrated that the values of LoD for Si, Mn, Cr, Ni, and V in molten steel were 107, 134, 649, 430, and 88 ppm, respectively, using calibration curves obtained with PLS model, with univariate calibration coefficient (R^2) greater than 0.99. In 2019, He et al. [108] proposed a genetic algorithm and backpropagation (BP) neural network model coupled with LIBS where carbon was detected in steel using C I 247.86 nm line instead of C I 193.09 nm line. To detect trace elements such as Mn, Cr, and Ni in steel, Zhang et al. [109] developed a new LIBS spectrum data treatment technique based on machine learning algorithms. The multivariate calibration curves of trace elements of interest demonstrated that the values of linearity fit (R^2) were within the range of 0.99966 to 0.99997, which was very close to unity. Relative error of prediction (REPs) and relative standard deviation (RSDs) for determining Mn, Cr, and Ni in steel was obtained in the range of 1.3–7.2% and 3.96–6.68%, respectively.

The conditions and LoD obtained in several studies of ferrous and nonferrous metals are summarized in Table 2.

4.2. Analysis of Foods. LIBS is one of the most promising optical tools for food quality control [117]. With increasing concerns placed recently for food quality and safety, LIBS demonstrates excellent potential for agricultural-related sample detection due to its rapid elemental detection capability [118].

Haider et al. [119] utilized SP-LIBS (Section 2.1) to analyze the micronutrients and ecotoxic elements in rice and husk samples from Bangladesh in which micronutrients such as Cu, Fe, Na, Mn, and Zn were found as well as the toxic trace element Cd. Kim et al. [120] applied SP-LIBS to quantify nutrients in unpolished rice, and LoDs of Mg, Ca, Na, and K were 7.54, 1.76, 4.19, and 6.70 ppm, respectively, as established from standard reference materials (SRMs). Luo et al. [121] employed SP-LIBS to analyze the effect of Cu stress on other elements such as Zn, Mn, Fe, Mg, Si, and K in rice husk. The study revealed that Zn, Mn, Fe, Si, and K concentrations are strongly correlated with Cu stress in rice husk.

Pérez-Rodríguez et al. [122] applied SD-LIBS (Section 2.3.3) with the SVM method for finding the origin of botanical rice where C, Ca, Fe, Mg, N, and Na lines were used as input variables for rice variety predictive modeling. Nespeca et al. [123] utilized an SD-LIBS system to analyze impurities in honey.

Sezer et al. [124] used the LIBS system coupled with mathematical methods (Section 2.4.3) to differentiate several types of meat regarding their differences in protein fractions (actin and myosin). Using the PLS model, LoDs for adulteration of beef with chicken and pork meat are 2.84 and 3.89%, respectively. In another paper, Guo et al. [125] applied sample set portioning on the joint x-y distance (SPXY) algorithm in conjunction with the SVM model and LIBS to differentiate five meat species. Zhao et al. [126]

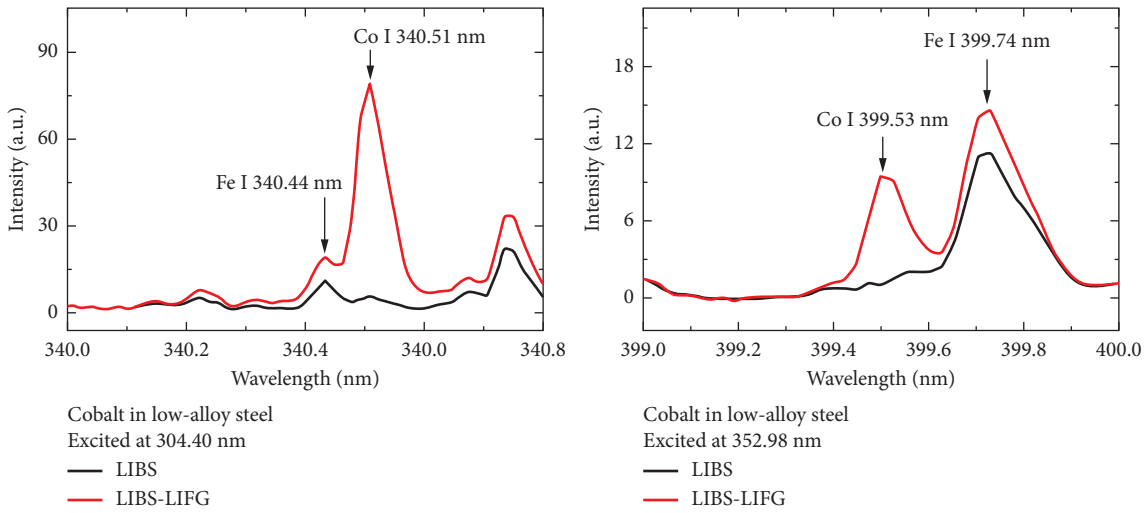

Figure 8: Comparison between LIBS-LIFG, LIBS-LIFE, and LIBS-only spectra for the low-alloy steel sample [101].

demonstrated that LIBS with PLSR modeling has better prediction performance and lower LoD (1079 ppm) than Raman and FT-IR with PLSR. In a similar study, Wang et al. [127] applied LIBS and the chemometrics method to determine the cadmium content in rice roots. Tian et al. [128] used the LIBS system with machine learning to evaluate the phosphorous concentration in seafood, and the LoD was estimated to be around 370 ppm for normalized data. Akın et al. [129] used the LIBS system with PLS regression to determine sorghum levels in flour mixtures consisting of corn and sorghum, and the corresponding LoD was 4.36%. Table 3 compiles different LIBS conditions and corresponding LoDs of trace elements in Food.

4.3. Micro- and Macronutrients Detection in Plants. LIBS coupled with an external electric field (Section 2.3.2) was introduced to enhance the emission intensity of Cr present in the *Euphorbia indica* plant [141]. The spectral lines of Cr appeared in the presence of the external electric field, while those were absent in LIBS-only spectra (Figure 9). LoD of Cr was found to be 4.8, 4.6, and 3.5 ppm in roots, stem, and leaf, respectively, using CF-LIBS methods. Similar experimental conditions and methods were applied to improve the emission signals of saline metals present in *Aerva javanica* plants [142]. In the presence of the external electric field line, intensities of Ca, Mg, K, and Na were enhanced by a factor of 7.9, 6.7, 1.3, and 2.97, respectively. The weighted concentration of the investigated elements (Ca, Mg, K, Na, Si, and Li) was determined in the range of 0.7 to 32 wt% and 0.5 to 33 wt% in the root and shoot samples, respectively. The electric field-assisted LIBS was also used to improve the LoD of Cu in the onion (*Allium cepa* L.) leaves [143], and the LoD of Cu was lowered up to 0.028 ppm.

Samek et al. [144] introduced an fs-LIBS (Section 2.2.2) for spectrochemical analysis of Fe in two leaf samples: dried maize and fresh *Cornus stolonifera*. Experimental results revealed that Fe concentrations as low as 5 ppm could be detected using this approach.

Seven heavy metals (As, Cd, Cr, Cu, Hg, Pb, and Zn) in *Sargassum fusiforme* (algae) were examined by Su et al. [145] using LIBS combined with the threshold variables-PLS model. Multivariate calibration method such as partial least square (PLS) is an empirical approach, that is, any knowledge of fundamental physical properties of plasma is not required [105]. These methods have been applied for the determination of nutrient profiles as well as toxic elements in plants [118, 146–149]. Nunes et al. [146] compared PLS with univariate calibration to detect nutrients in sugarcane leaves. The PLS method demonstrated better root-mean-square error prediction (RMSEP) values than univariate calibration for all the investigated elements except K and Mn. By the PLS model, LoDs of P, K, Ca, Mg, Mn, Fe, Zn, and B obtained were 0, 210, 80, 120, 6.6, 1.2, and 0.8 ppm, respectively. Likewise, Braga et al. [149] reported that for analysis of different plant materials, LoDs of all the elements of interest (B, Cu, Fe, and Mn) except Zn were improved in the PLS approach and varied from 3 to 12 ppm. Yao et al. [118] used the PLS method to enhance the prediction accuracy of Cd in polluted fresh leafy vegetables. Peng et al. [147] applied LIBS combined with multivariate calibration based on PLS to detect Cr in rice leaves. Relatively high LoDs were achieved for nutrients in plant materials when an fs-LIBS is used in conjunction with PLS [148], and the LoDs of Ca, Mg, P, Cu, Fe, Mn, and Zn were 0.007, 0.02, 0.4, 7, 12, 2, and 80 ppm, respectively. To enhance accuracy in the detection of heavy metals in mulberry leaves, Yang et al. [150] proposed a novel analysis framework consisting of a self-organizing map (SOM), successive projection algorithm (SPA), and uninformative variable elimination (UVE). LIBS was combined with chemometrics for quick and accurate quantitative analysis of heavy metal Cd in rice stems [151] and roots [127]. Table 4 summarizes the different works related to detecting nutrients and toxic elements in plants by LIBS.

4.4. Trace Element Detection in Biomaterials. Roldán et al. [155] applied the combination of LIBS and neural networks

Table 2: LIBS characterization of the trace elements in different ferrous and nonferrous metals.

Method	Operating parameters	Matrix	Element	LoD (ppm)	Year	Ref No.
LIBS	Q-switched Nd:YAG, 1,064 nm, 8 ns, 200 mj, 20 Hz	Steel	C	65	1992	[110]
Multiple-laser pulse	Q-switched Nd:YAG, 1,064 nm	Low alloy steel	C	7	2000	[111]
Multiple-laser pulse	Q-switched Nd:YAG, 1,064 nm	Liquid steel	C	5	2003	[112]
LIBS	Q-switched Nd:YAG, 532 nm, 6 ns, 160 mj, 10 Hz	Steel	C	5	2001	[113]
DP VUV LIBS	Q-switched Nd:YAG, 1,064 nm, 15 ns, 200 mj	Steel	C	2.9 (N_2)	2014	[90]
LIBS-LIRF	Q-switched Nd:YAG, 532 nm, 6 ns, 2 mj, 10 Hz	Steel	C	130 (N_2), 390 (air)	2017	[114]
LIBS	Q-switched Nd:YAG, 1,064 nm, 7 ns, 200 mj, 20 Hz	Steel	S	70	1995	[115]
Multiple-laser pulse	Q-switched Nd:YAG, 1,064 nm	Low alloy steel	S	8	2000	[111]
Multiple-laser pulse	Q-switched Nd:YAG, 1,064 nm	Liquid steel	S	11	2003	[112]
LIBS	Q-switched Nd:YAG, 532 nm, 6 ns, 160 mj, 10 Hz	Steel	S	4.5	2001	[113]
DP VUV LIBS	Q-switched Nd:YAG, 1,064 nm, 15 ns, 200 mj	Steel	S	1.5 (N_2)	2014	[90]
Multiple-laser pulse	Q-switched Nd:YAG, 1,064 nm	Low alloy steel	P	9	2000	[111]
Multiple-laser pulse	Q-switched Nd:YAG, 1,064 nm	Liquid steel	P	21	2003	[112]
LIBS	Q-switched Nd:YAG, 532 nm, 6 ns, 160 mj, 10 Hz	Steel	P	6	2001	[113]
LIBS-LIF	Q-switched Nd:YAG, 532 nm, 6 ns, 10 Hz	Steel	P	0.7	2009	[99]
LIBS	Q-switched Nd:YAG, 532 nm, 6 ns, 160mj, 10 Hz	Steel	N	15–25	2001	[113]
Multiple-laser pulse	Q-switched Nd:YAG, 1,064 nm	Liquid steel	Cr	9	2003	[112]
DP LIBS + PLS	Q-switched Nd:YAG, 1,064 nm, 7 ns, 10 Hz	Molten steel	Cr	649	2015	[106]
Multiple-laser pulse	Q-switched Nd:YAG, 1,064 nm	Liquid steel	Ni	9	2003	[112]
DP LIBS + PLS	Q-switched Nd:YAG, 1,064 nm, 7 ns, 10 Hz	Molten steel	Ni	430	2015	[106]
LIBS + ring magnet confinement	Q-switched Nd:YAG, 532 nm, 5 ns, 60 mj.	Steel	V	11	2014	[98]
DP LIBS + PLS	Q-switched Nd:YAG, 1,064 nm, 7 ns, 10 Hz	Molten steel	V	88	2015	[106]
LIBS + ring magnet	Q-switched Nd:YAG, 532 nm, 5 ns, 60 mj.	Steel	Mn	30	2014	[98]
DP LIBS + PLS	Q-switched Nd:YAG, 1,064 nm, 7 ns, 10 Hz	Molten steel	Mn	134	2015	[106]
DP LIBS + PLS	Q-switched Nd:YAG, 1,064 nm, 7 ns, 10 Hz	Molten steel	Si	107	2015	[106]
LIBS-LIF	Q-switched Nd:YAG, 532 nm, 6 ns, 50 mj, 10 Hz	Low alloy steel	Co	0.82	2016	[101]
LIBS-LIF	Q-switched Nd:YAG, 532 nm, 8 ns, 60 mj, 10 Hz	Steel	B	0.5	2016	[100]
RELIBS	Q-switched Nd:YAG, 1,064 nm, 7 ns, 5 Hz	Aluminum alloy	Mg	21	2010	[44]
RLIBS	OPO laser, 210 nm–2.2 μm, 20–200 μj, 5 ns, 10 Hz	Aluminum alloy	Mg	0.75	2013	[45]
DP-LIBS	Q-switched Nd:YAG, 1,064 nm, 30 mj, 12–13 ns, 1 Hz	Aluminum alloy	Cr	10	2006	[93]
DP-LIBS	Q-switched Nd:YAG, 1,064 nm, 60 mj, 8 ns, 10 Hz	Aluminum alloy	Sr	0.56	2018	[94]
RELIBS	Q-switched Nd:YAG, 1,064 nm, 7 ns, 5 Hz	Aluminum alloy	Si	1438	2010	[44]
RLIBS	OPO laser, 210 nm–2.2 μm, 20–200 μj, 5 ns, 10 Hz	Aluminum alloy	Si	80	2013	[45]
DP-LIBS	Q-switched Nd:YAG, 1,064 nm, 5 ns	Aluminum alloy	Li	3.2	2019	[95]
CF-LIBS	Q-switched Nd:YAG, 1,064 nm, 80–120 mj, 5 ns, 10 Hz	Gold alloy	Ag	4.3	2018	[116]
CF-LIBS	Q-switched Nd:YAG, 1,064 nm, 80–120 mj, 5 ns, 10 Hz	Gold alloy	Au	0.05	2018	[116]
LIBS-LIF	Q-switched Nd:YAG, 532 nm, 8 ns, 60 mj, 10 Hz	Nickel-based superalloy	B	0.9	2016	[100]

Table 3: LIBS conditions and corresponding LoDs of trace elements in foods.

Method	Description of laser	Sample materials	Trace element	LoD (ppm)	Reference
LIBS	Q-switch Nd:YAG laser, 1,064 nm, 650 mJ, 7 ns, 10 Hz	Spinach	Mg II	29.63	[120]
			Ca I	102.65	
			Na I	36.36	
			K I	44.46	
		Unpolished rice	Mg II	7.54	
			Ca I	1.76	
			Na I	4.19	
			K I	6.70	
LIBS and ICP-MS	Q-switch Nd:YAG laser, 266 nm, 8 ns, 15~18 mJ, 10 Hz	Dates	Mg I	6	[130]
			Ca I	17	
			Cr I	1	
LIBS	Q-switch Nd:YAG laser, 1,064 nm, 40 mJ, 8 Hz, 650 ns, 1.05 ms	White chickpea	Ti	33.9	[131]
LIBS	Q-switch Nd:YAG laser, 1,064 nm, 0~100 mJ,: 0~2 μs, 50~250 μm, 5 Hz	Flour samples	Ca	45–80	[132]
			K	105–200	
			Mg	25–60	
LIBS and ICP-MS	Q-switch Nd:YAG laser, 266 nm, 30 mJ, 8 ns, 20 Hz	Tea samples	Fe	22	[133]
			Cr	12	
			K	14	
			Br	11	
			Cu	6	
			Si	1	
LIBS and EDXRF	Q-switch Nd:YAG laser, 1,064 nm, (365 ± 3) mJ, 5 ns	Wheat flour	Ca	12	[134]
			P I	40	
			K I	1200	
			Ca II	17	
			Mg I	10	
			Fe II	0.7	
			Mn II	0.5	
			Zn II	1.0	
			Cu I	0.5	
Nanoparticle-enhanced LIBS	Q-switch Nd:YAG laser, 1,064 nm, 160 mJ, 3–5 ns, 0.2 μs	Fruits and vegetables	PI (213.62 nm)	0.019	[135]
			PI (214.91 nm)	0.015	
			PI (253.56 nm)	0.009	
			PI (255.33 nm)	0.029	
			Cd I (214.4 nm)	0.0016	
LIBS	Q-switch Nd:YAG laser, 1,064 nm, 950 mJ, 5 ns, 2.0 μs, 1~10 Hz	Cucurbit seeds (pumpkin, ash gourd, watermelon, muskmelon)	Mg II	5, 12, 3.4, 3.2	[136]
			Ca II	26.6, 35.8, 18.1, 28.2	
			Na I	44.2, 43.9, 47.9, 36.8	
			K I	21.9, 21.1, 29.3, 37.9	
LIBS	Q-switch Nd:YAG laser, 532 nm, 1 Hz, 14 mJ/pulse, 1 Hz	Bakery products (bread)	Nacl	175	[137]
			Na	69	
LIBS	Q-switch Nd:YAG laser, 1,064 nm, 150 mJ, 5 ns	Infant formula	Ca	3,690	[138]
LIBS	Q-switch Nd:YAG laser, 1,064 nm, 50 mJ, 8 ns	Breakfast cereals	Ca	9.5	[139]
LIBS	Q-switch Nd:YAG laser, 1,064 nm, 400 mJ, 8 ns, 10 Hz	Mochi (Japanese rice cake)	Cu	0.1	[140]

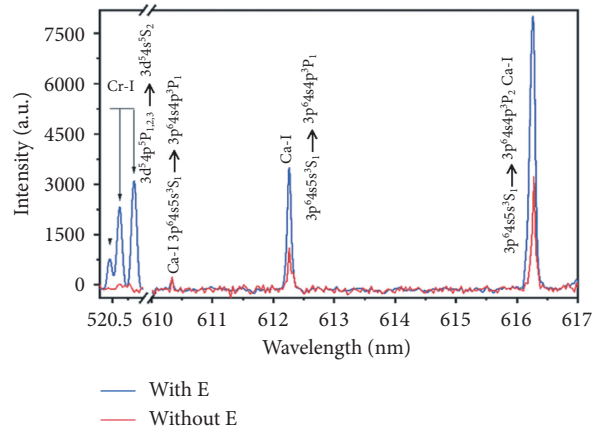

Figure 9: LIBS spectra of *Euphorbia indica* root with and without the electric field (adapted from [141]).

Table 4: LIBS characterization for the detection of nutrients and toxic elements in plants.

Method	Operating parameters	Matrix	Elements	LoD (ppm)	Year	Ref No.
Univariate calibration	Nd:YAG laser, 1,064 nm, 2 μs, 200 mj, 10 Hz	Leaves of soya, lettuce, endive, boldo, grass, jack, brachiaria, coffee, mango, maize, and pepper	B, Cu, Fe, Mn, Zn	1.4, 2.5, 2.8, 1.1, 1.0	2008	[152]
Univariate calibration	Nd:YAG laser, 1,064 nm, 2 μs, 10 Hz	Sugar cane leaves	Ca, Mg, P, B, Cu, Fe, Mn, Zn, al, K	0.1, 0.01, 1.0, 0.5, 0.4, 0.4, 0.3, 0.2, 3.9, 2,000	2012	[153]
Univariate calibration	Nd:YAG laser, 1,064 nm, 2 μs, 200 mj, 10 Hz	Leaves and flowers of cannabis	Al, Ba, Ca, Br, Cu, Fe, K, Mg, Mn, Na, P, Rb, Sr	4.7, 0.22, 69.4, 0.11, 0.12, 1.65, 158, 14.9, 3.01, 1.4, 22, 0.1, 0.8	2015	[154]
Univariate calibration	Fs-laser, 795 nm, 160 fs, 100 μj, 10 Hz	Dried maize and fresh *Cornus stolonifera*	Fe	Not reported	2005	[144]
Univariate calibration	Nd:YAG laser, 1,064 nm, 80 and 140 mj, 10 Hz	Spinach leaves and unpolished rice	Mg, Ca, Na, K	29.63, 102.65, 36.36, 44.46 (spinach leaves), 7.54, 1.76, 4.19, 6.7 (rice)	2012	[120]
Univariate calibration	Nd:YAG laser, 532 nm, 5 ns, 500 mj, 10 Hz	*Allium cepa* L. leaves	Cu	0.028	2019	[143]
PLS	Nd:YAG laser, 1,064 nm, 2 μs, 110 mj, 10 Hz	Sugarcane leaves	P, K, Ca, Mg, Mn, Fe, Zn, B	30, 210, 80, 120, 6.6, 9.5, 1.2, 0.8	2010	[146]
PLS	Nd:YAG laser, 532 nm, 1.1 μs, 70 mj, 10 Hz	Leaves of brachiaria, soya, banana, coffee, maize, mango, pepper	B, Cu, Fe, Mn, Zn	3, 5, 7, 4, 12	2010	[149]
PLS	Ti:sapphire laser, 800 nm, 35 μs, 1.65 mj, 1 kHz	Leaves of sugar cane, soya, citrus, coffee, maize, bean, eucalyptus, mango, banana, grape, millet, rubber tree, tomato	Ca, Mg, P, Cu, Fe, Mn, Zn	7, 20, 400, 7, 12, 2, 80	2015	[148]
Univariate and PLS	Nd:YAG laser, 532 nm, 4 and 20 μs, 60 mj, 1 Hz	Rice leaves	Cr	4.3856 (univariate calibration)	2017	[147]
CF-LIBS	Nd:YAG laser, 1,064 nm, 5 μs, 850 mj, 10 Hz	Roots, stem, and leaves of *Euphorbia indica*	Cr	4.8 (root), 4.6 (stem), 3.5 (leaf)	2019	[141]

to determine the elemental composition of bones for differentiating wild deer bones from different individuals. Detected elements were P, Mg, Ca, Ba, and Sr. Moncayo et al. [156] used LIBS and neural networks (NN) to differentiate peoples by analyzing their bones and teeth fragments collected from the graveyard. In a recent study, Siozos et al. [157] applied LIBS with NN analysis to assign seventeenth- to nineteenth-century archaeological bone remains to individuals using elemental information of bone remains. Gomes et al. [158] used the one-point calibration-laser-

induced breakdown spectroscopy (OPC-LIBS) for the elemental analysis of bioactive ceramic (hydroxyapatite), which has human bone-like composition and crystalline structure. In addition, an important ratio (Ca/P) has been studied to know about the final deposition stoichiometry of that material. Martinez and Baudelet [159] used the LIBS system to analyze human nails to measure the concentration of zinc.

Samek et al. [160] applied LIBS with the Mahalanobis distance pattern recognition algorithm to identify unknown tooth samples in real time. Using the two lines of Mg (518.36 nm) and Ca (518.89 nm), the intensity ratio can be used to identify the healthy tooth from carious ones. If $(I_{Ca}/I_{Mg}) > 4.3$, it can be considered a healthy tooth. Ahmed et al. [161] applied LIBS and found that P, Na, and Ca concentrations are higher in healthy portions than carious parts of deciduous teeth (baby teeth).

Rehse et al. [162] applied the LIBS system to study the growth of "*Pseudomonas aeruginosa*" bacteria in blood and bile. In their work, calcium, magnesium, and sodium were detected and utilized to distinguish the bacteria. Samuels et al. [163] employed the LIBS technique to discriminate the bacterial spores, molds, pollens, and proteins. Dell'Aglio et al. [164] investigated the possible application of NELIBS as a sensing tool where AuNP-protein (such as human serum albumin or cytochrome C) solution is deposited on a metallic titanium substrate. The maximum enhancement of Ti line intensity was observed when nanoparticle-protein corona is formed, and the corresponding number of protein units needed to construct the corona can be estimated.

Haider and Khan [165] performed SP-LIBS on the corals (the skeleton of dead microorganisms), and several elements such as Ca, C, Sr, Na, Mg, Li, Si, Cu, Ti, K, Mn, Zn, Ba, Mo, Br, and Fe were detected (Figure 10). Muhammed Shameem et al. [50] utilized LIBS-Raman (Section 2.4.1) to determine the constituent elements at renal calculi. LIBS has been used by Singh et al. [166] to classify gallbladder stones by using their constituents elements.

4.5. Analysis of Pigments and Other Archeological Samples. Cristoforetti et al. [167] applied the LIBS-Raman technique to identify pottery elements and analyze the molecular structure of the pigments in pottery samples collected from the northern part of Syria. PCA was applied by Osticioli et al. [168] to identify and differentiate between natural and synthetic ultramarine blue pigments using LIBS-Raman (2.4.1). Spectral analyses showed that Al, Na, and Si were found in all the pigment samples. Natural and artificial ultramarine blue pigments were differentiated based on calcium content since Ca was absent in synthetic pigments.

In another paper, Lazic et al. [169] applied LIBS-LIF (Section 2.3.1) to find the pigment's elemental composition on the surface of Renaissance Umbrian pottery. LIBS has done semiquantitative analysis on all the ceramic layers, and Al, Ca, Cu, Fe, Mg, Na, Si, Sn, and Pb were detected.

Studies revealed that the LIBS technique could successfully identify organic and inorganic materials with high precision and accuracy. Another advantageous feature of LIBS is that each laser pulse can uncover a new part of the paint layer by removing a tiny amount of surface materials [170].

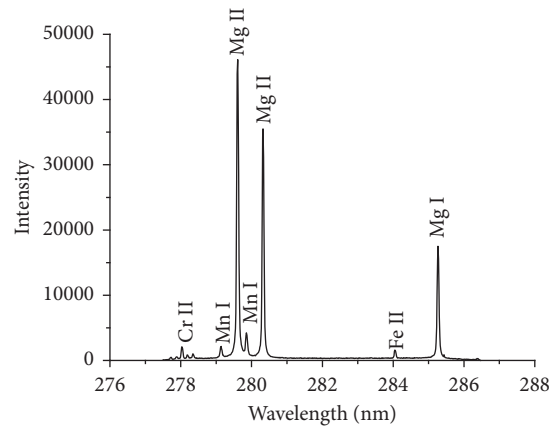

Figure 10: The SP-LIBS spectrum of a coral skeleton with identified trace elements, collected from Inani Beach, Cox's Bazar [165].

4.6. Detection of Explosive Residues. The handling and transportation of explosives have been shown to generate traces of explosives on surfaces [171]. The first demonstration of detecting explosives using LIBS (Figure 11) was done by De Lucia et al. [172]. Although the sensitivity of LIBS is much less than that of vapor-based techniques, which typically have LoD of the order of ppt [173], the major advantage of LIBS is its ability for real-time, stand-off detection for safety purposes (up to 130 m has been achieved) [174]. However, for stand-off detection of the explosive residue by LIBS, the high power of lasers is hazardous for the human eye. The limitation for LIBS is that the explosive detection is restricted only to the beam path.

Different multivariate chemometric techniques have been used for the discrimination of energetic material, such as PCA, PLS discriminant analysis [175], SIMCA, and neural networks. Among them, the most promising chemometric-based approach was found to be PLS-DA. In general, a "training set" is built from many LIBS spectra, which serves as a standard in chemometric-based approaches. Then the number of dimensions in the data provided in the training sets is decreased. Therefore, intricacy is also reduced, and new data can be matched accurately [176].

DP LIBS demonstrates an increase in the emission signal of explosive residues. In DP LIBS, the first pulse is efficiently absorbed, and a successive second pulse would efficiently reheat the plasma [173, 177]. Gottfried et al. [178] analyzed RDX and a mixture of 36% TNT, 63%RDX, and 1% wax (termed Composition-B) using double-pulse LIBS, and they were able to detect the simulants at 20 m using PCA as a chemometric technique. In another work, Gottfried et al. [175] investigated RDX, Composition-B, and TNT using the same experimental setup. However, in this case, they reported the identification of explosive residues even when mixed with dust.

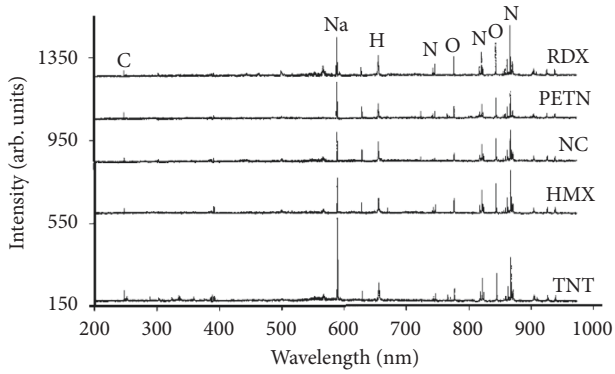

Figure 11: LIBS spectra of different types of pure explosive compounds (adapted from [172]).

Another way to improve the detection of explosive residue is fs-LIBS (Section 2.2.2) that minimizes background continuum and atmospheric entrainment, which are experimentally demonstrated by De Lucia et al. [26] using RDX, C-4, and Composition-B explosives residue deposited on aluminum substrates.

4.7. Detection of Rare Earth Elements (REEs). Most of the reported REEs detection by LIBS are linked with detecting a few elements in lab-prepared or commercially available samples of lanthanide compounds. Bhatt and coworkers [179] performed univariate and multivariate analyses of six REEs (Ce, Eu, Gd, Nd, Sm, and Y) and obtained calibration curves for these REEs. LoDs are found to be 0.098, 0.052, 0.077, 0.047, 0.250, and 0.036%, for Ce, Eu, Gd, Nd, Sm, and Y, respectively. Castro et al. [180] demonstrated the direct determination of Dy, Gd, Nd, Pr, Sm, and Tb in hard disk magnets by SP-LIBS. The concentrations of some REEs such as Ho, Er, and Pr in LiCl + KCl eutectic salt matrices were measured by SP-LIBS through a quartz window atop an airtight sample cell containing argon gas [181]. Martin et al. [182] used SP-LIBS for the detection of Eu, Gd, La, Nd, Pr, Sm, and Y, where a microscope objective was used to focus the laser on the mixture of 5% oxide and 95% graphite matrix, and an innovative collection optics are used to collect the plasma's emission. In another paper, Tampo et al. [183] used antenna-coupled MA-LIBS and observed 50-fold enhancement in the emission intensity of gadolinium ions. The observed detection limit of the MA-LIBS was found to be 40 ppm.

Whereas most of these works are associated with the detection of REEs in commercially available samples, Abedin et al. [184] reported the first multiple rare earth (Ce, La, Pr, Nd, Y, Yb, Gd, Dy, and Er) detection in a naturally occurring monazite mineral by SP-LIBS (Figure 12). Likewise, Haider and Khan [185] detected multiple rare earth (Ce, La, Pr, Nd, Yb, Gd, Dy, Er, Sm, Eu, Ho, and Y) in an enriched zircon sample by SP-LIBS. The same group also identified trace REEs (Nd, Yb, Sm, Ce, Dy, and Gd) in coal samples collected from coal mines of Bangladesh (Barapukuria) and India (Meghalaya) [186]. LIBS can measure REE contents in geological minerals and ores and provide results comparable to ICP-MS analysis. In natural geological samples, Bhatt et al. [187] employed SP-LIBS to detect and quantify REEs (Ce, La, Nd, Y, Pr, Sm, Eu, Gd, and Dy). For the quantification of Ce, La, and Nd, multivariate analysis was executed by developing PLS regression models. Using SP-LIBS as a drill core scanner, Müller et al. [188] analyzed thin sections of drill core of the geological material Storkwitz carbonatite, and the presence of Ce, La, and Nd were detected.

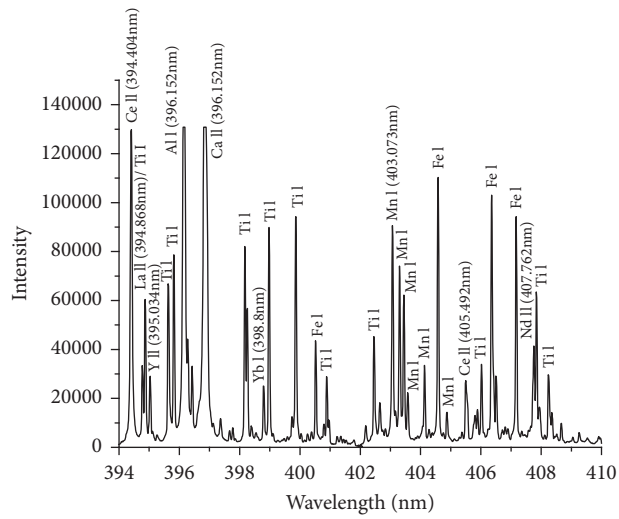

Figure 12: SP-LIBS spectrum for monazite sands along with some identified lines for REEs (adapted from [184]).

Bhatt et al. [21] used DP-LIBS (pulses wavelength 1,064 nm) in a collinear configuration to demonstrate enhancement of the signal intensity of Eu, Gd, Pr, and Y using Eu_2O_3, Gd_2O_3, Pr_2O_3, and Y_2O_3 pellets, respectively. In another work, employing LIBS-LIF, Shen and coworkers [189] have demonstrated the detection of U as low as 462 ppm in glass samples [16].

4.8. Detection of Trace Elements by Liquid-to-Solid Conversion. The trace element concentration can be increased significantly using a suitable adsorbent, and this liquid-to-solid conversion of samples is advantageous for more accessible and inexpensive detection of trace and toxic elements. For example, Haider et al. [15] employed the LIBS combined with adsorption for the sensitive detection of arsenic in water (Figure 13). In this study, two adsorbents, ZnO and charcoal, were employed to improve the emission line's intensity. As an adsorbent of arsenic, ZnO provided better results than charcoal. A LoDs of 1 ppm was achieved using ZnO, while that of the charcoal was 8 ppm. It was also reported that a concentration of arsenic as low as 0.083 ppm in water was detected using preconcentration of the liquid sample and adsorption techniques.

Chen et al. [70] used wood slices as a liquid absorber in the LIBS experiment for rapid and sensitive detection of toxic heavy elements such as Cr, Cd, Pb, Mn, and Cu in water. In this study, LoD was obtained in the range of 0.029–0.59 ppm, which was 2–3 orders lower than the results obtained by direct LIBS analysis on an aqueous solution. On the other hand, Youli et al. [190] used ordinary printing

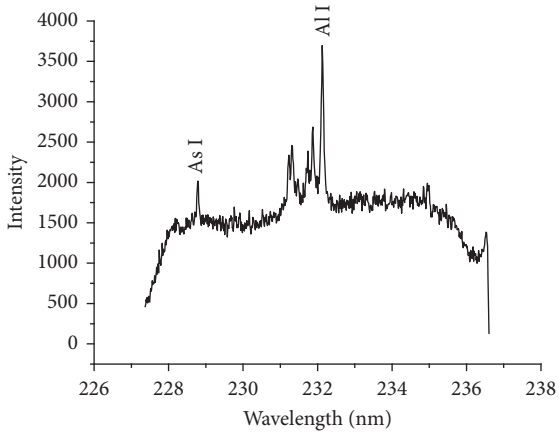

Figure 13: LIBS spectrum of adsorption coupled LIBS reported to detect arsenic in 7 ppm aqueous solution (adapted from [15]).

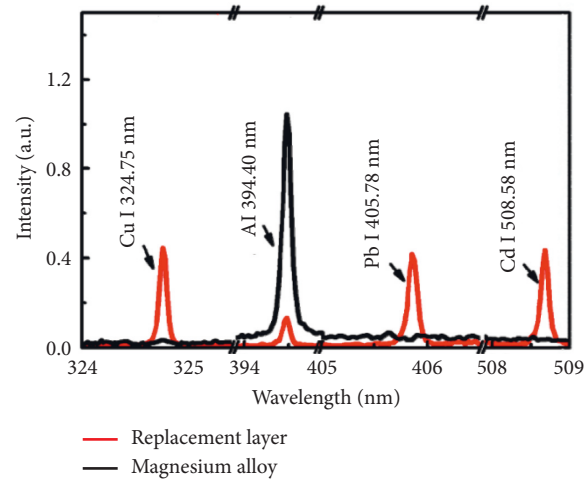

Figure 14: LIBS spectra of magnesium alloy (solid black line) and replacement layer (solid red line) from mixed solutions of different salts ($CrCl_3$, $CdCl_2$, $CuCl_2$, and $Pb(NO_3)_2$; adapted from [80]).

paper as a liquid absorber. In this experiment, the LoD of Cr and Pd was 0.026 and 0.033 ppm, respectively, which was a slight improvement compared to the previous one where the wood slice was used as an absorber.

To enhance the detection sensitivity of LIBS for Cd content determination in drinking water, Tian et al. [191] employed a water purifier chelating resin ECS60 as the enrichment matrix. Chelating resin has a rough and porous surface, which helps it adsorb heavy metals effectively. A comparison of resin and filter paper as an adsorbent was investigated, and the results confirmed that chelating resin was more efficient than filter paper. The LoD was 0.0036 ppm, which met the sanitation standard of drinking water in China. So LIBS coupled with chelating resin ECS60 could be a safe, low-cost, and rapid method for monitoring drinking water quality. LIBS was utilized to determine boron in sub-ppm concentrations in groundwater employing graphite planchets as solid support [192]. The LoD in groundwater was found to be 0.01 ppm by using the 249.773 nm atomic line for boron.

In contrast to these adsorption methods, Zhao et al. [193] used SP-LIBS coupled with an electrical-deposition method to analyze the trace heavy metal ions in tap water. A rotating cathode system was designed to deposit the trace metals on the surface of the cathode material. An aluminum rod having high purity was selected as a cathode because it can enhance the deposition homogeneity of the metal ions and reduce the generation of gas bubbles in the electrical deposition process. Trace heavy metal ions, such as Cr^{3+}, Mn^{2+}, Cu^{2+}, Zn^{2+}, Cd^{2+}, and Pb^{2+} were quantitatively analyzed in the tap water samples with an LoD of $1.6\times10^{-4}-1.35\times10^{-3}$ ppm. These were 5–6 orders of magnitude better than the results obtained by direct tap water analysis by LIBS and 2–3 orders better than using wood slice substrates. Chen et al. [75] also used the SP-LIBS technique coupled with an electrical-deposition method to analyze the trace heavy metal ions in water. Cr^{3+}, Mn^{2+}, Cu^{2+}, Zn^{2+}, Cd^{2+}, and Pb^{2+} trace heavy metal ions were quantitatively analyzed in the tap water samples with an LoD of $8.3\times10^{-5}-5.6\times10^{-3}$ ppm. These were 5–6 orders better than the results produced by the analysis in water by conventional LIBS.

To lower the LoD of Pb and Cr in drinking water, Ma et al. [78] used SENLIBS (2.5.2), where the effect of four substrates (Zn, Mg, Ni, and Si) was compared. Among the four substrates, Zn showed the best result. LoD was 0.0011 and 0.004 ppm for Cr and Pb, respectively, using a Zn substrate, which was lower than the sanitation standard of the drinking water in China (0.05 ppm for Cr and 0.01 ppm for Pb). The chronology of LoD of Cr and Pb using several substrates is in the sequence of Zn > Mg > Ni > Si, while LoD is correlated with the boiling point of the substrate. The detection sensitivity of heavy metals in water was better for a substrate of a lower boiling point as the amount of ablation of the target is inversely related to the boiling point. So, with the decrease of the boiling point, the content of the matrix increased, resulting in an intense collision between particles and increased electron density and plasma temperature. Consequently, spectral lines of higher intensity and improved LoD were observed. Zhang et al. [194] studied the impact of substrate temperature on the detection sensitivity of SENLIBS technology. Observed LoDs of Cr and Pb were 0.0046 and 0.0317 ppm, respectively, at 25°C. It was improved up to 0.0012 and 0.008 ppm when the substrate temperature reached 200°C.

Yang et al. [80] introduced chemical replacement coupled with the surface-enhancement LIBS (CR-SELIBS) method to overcome the poor detection sensitivity of LIBS in water. In this method, cleaned magnesium alloy was immersed into the aqueous solution containing heavy toxic metals and then dried. As a result of the chemical replacement reaction, Cu, Pb, Cd, and Cr in the liquid sample were enriched on the surface of the magnesium alloy (Figure 14), and an average thickness of 2 μm was reported. LoDs of the toxic metal ions were in the range of 0.016–0.386 ppm.

For improving the detection sensitivity of Cl and S in water solution, a novel technique termed indirect LIBS (ID-LIBS) was introduced by Ma et al. [195]. In ID-LIBS, Cl was

Table 5: LIBS characterization of the trace elements in drinking water.

Method	Operating parameters	Matrix	Trace element	LoD (ppm)	Year	Reference
LIBS + liquid jet	Q-switch Nd:YAG laser, 1,064 nm, 6 ns, 150 mj, 5 Hz	Water	Pb, Cd	4, 68	2011	[201]
LIBS + liquid jet	Q-switch Nd:YAG laser, 532 nm, 4 ns, 425 mj, 1–10 Hz	Water (unitary matrix)	Cr	1.1	2008	[202]
LIBS + aerosol	Q-switch Nd:YAG laser, 532 nm, 10 ns, 45–150 mj, 10 Hz	Water	Cr, Pb, Cd	6.49, 13.6, 43.99		[203]
Single-pulse LIBS	Q-switch Nd:YAG laser, 1 ns, 100 mj, 1 Hz	Ice and water	Cd, Fe, Mg, Cr, Cu, Hg, Pb	1.4, 1.3, 0.3, 1.4, 2.3, 3.7, 1.3 (ice), 7.1, 10.5, 0.9, 10.5, 9.6, 21.4, 12.5 (water)	2012	[204]
Single-pulse LIBS + wood	Q-switch Nd:YAG laser, 1,064 nm, 12 ns, 100 mj, 5 Hz	Water	Cr, Cu, Cd, Pb	0.034, 0.029, 0.59, 0.074	2008	[70]
Single-pulse LIBS + printing paper	Q-switch Nd:YAG laser, 1,064 nm, 10 ns, 100 mj, 1 Hz	Water	Cr, Pb	0.026, 0.033	2014	[190]
Single-pulse LIBS + four substrates (Zn, Mg, Ni, and Si)	Q-switch Nd:YAG laser, 532 nm, 7 ns, 3 mj, 10 Hz	Drinking water	Cr, Pb	0.0011 (Zn), 0.0022 (Mg), 0.0038 (Ni), 0.0041 (Si) (Cr), 0.004 (Zn), 0.012 (Mg), 0.021 (Ni), 0.024 (Si) (Pb)	2019	[78]
ID-LIBS	Q-switch Nd:YAG laser, 532 nm, 7 ns, 3 mj, 10 Hz	Water	Cl, S	2, 5	2020	[195]
Single-pulse LIBS + adsorption (chelating resin ECS60)	Q-switch Nd:YAG laser, 1,064 nm, 3–5 ns, 200 mj, 20 Hz	Drinking water	Cd	0.0036	2019	[191]
Single-pulse LIBS + adsorption (ZnO and Charcoal)	Q-switch Nd:YAG laser, 532 nm, 8 ns, 40 mj, 10 Hz	Ground water	As	1.0 (ZnO), 8.0 (charcoal)	2014	[15]
LIBS-LIF + wood	Q-switch Nd:YAG laser, 532 nm, 12 ns, 8mj, 5 Hz	Water	Cu	0.0036	2019	[200]
Single-pulse LIBS + electrical-deposition (Al)	Q-switch Nd:YAG laser, 1,064 nm, 12 ns, 50 mj, 5 Hz	Water	Cr, Mn, Cu, Zn, Cd, Pb	0.000572, 0.000374, 0.000083, 0.0056, 0.000528, 0.000518	2008	[75]
Single-pulse LIBS + electrical-deposition (Al)	Q-switch Nd:YAG laser, 1,064 nm, 12 ns, 60 mj	Tap water	Cr, Mn, Cu, Zn, Cd, Pb	0.000317, 0.000176, 0.000162, 0.00135, 0.000787, 0.00057	2010	[193]
CR-SELIBS	Q-switch Nd:YAG laser, 532 nm, 5 ns, 50 mj, 5 Hz	Water (unitary matrix)	Cu, Pb, Cd, Cr,	0.257, 0.136, 0.386, 0.016	2016	[80]
Biomimetic array LIBS	Q-switch Nd:YAG laser, 1,064 nm, 13 ns, 100 mj, 1 Hz	Water	Pb, Sr, Ba, Cr, Cu, Cd, Be, Mn	0.00148,0.0000083, 0.000065, 0.00012, 0.000059, 0.00017, 0.0135, 0.000073, 0.00032	2021	[205]
LIBS	Q-switch Nd:YAG laser, 1,064 nm, 20 mj, 10 Hz	Water	F, Cl	0.38, 1.03	2021	[196]
SE-LIBS	Q-switch Nd:YAG laser, 1,064 nm, 10 ns, 20 mj, 1 Hz	Water	Pb, Cr	0.0317, 0.0046 (25°C) 0.008, 0.0012 (200°C)	2021	[194]

indirectly detected by AgCl, that is, from the precipitation reaction of Ag and Cl and subsequent separation by centrifugation, whereas S was detected by $BaSO_4$ precipitation. Tang et al. [196] proposed LIBS assisted with molecular emission for sensitive detection of F and Cl in water solution. The LoDs of F and Cl were 0.38 and 1.03 ppm, respectively.

Ma et al. [197] analyzed the effect of pH on detecting Cr and Cd in wastewater using LIBS-PT (Section 2.5.1). They observed that at low pH, the production of salt floccule occurs when an acid reacts with a metal, thereby reducing the spectral enhancement obtained through LIBS-PT on the surface of a metallic substrate. Ahmed et al. [11] allowed

surface water (river water) around Dhaka to settle down in a container, and the accumulated residues at the bottom were dried to form pellets, enabling the identification of toxic trace element Cr by SP-LIBS. In a similar work by Haider et al. [198], Cr, Co, and Ni were detected in water samples collected from different water bodies around Dhaka city in Bangladesh.

Remarkably, several reports have demonstrated LoD in the tens of ppb to a few ppb levels. To achieve a detection limit down to the ppb level, Kiris et al. [199] employed a transversely excited atmospheric (TEA) CO_2 laser, and a drop of analyte solutions is dried after deposition on Polytetrafluoroethylene (PTFE) substrate. The LoDs as low as 0.0053, 0.033, 0.32, and 0.12 ppm for Be, Cr, Pb, and Tl are obtained, respectively. However, they observed that the predeposition of copper oxide NP on the substrate, as typically done in NELIBS, does not improve the analytical performance. On the other hand, in the case of an Nd:YAG laser, predeposition of copper oxide NPs enhances the performance, and this NELIBS technique provides LoDs for Be, Cr, Ni, Co, and V to 0.0042, 0.1, 0.4, 0.35, and 0.20 ppm, respectively. Sensitive detection of Cu in water solution was reported by Wang et al. [200], taking advantage of the LIBS-LIF technique and using wood as an absorber. The LoD was found to be five orders lower than that obtained in the direct LIBS technique of liquid matrix, and it was as low as 0.0036 ppm.

The conditions and key findings obtained in several studies on detecting trace elements in water are summarized in Table 5.

5. Conclusion

LIBS-coupled techniques have emerged as a promising and effective tool for the spectrochemical analysis of trace elements, whereas conventional LIBS has poor performance. This review reports the state of the art of different LIBS-coupled techniques, and the recent use of these techniques in the elemental analysis is presented. The outstanding improvement of these techniques' analytical performance for trace element detection is also highlighted. Modification of LIBS (e.g., using double pulse) or the combination of LIBS with a secondary energy source (laser, microwave, or magnetic/electric field) is an efficient approach to improve the emission signal of plasma plume and can significantly lower the LoDs. Selective excitation in the LIBS-LIF system can solve the complex spectral interferences that impede trace element detection. Integrating LIBS with Raman in a single piece of equipment can improve proficiency in detecting trace elemental content by delivering complementary data. The chemometric-based approaches have proven promising for sample classification of rock, mineral, or alloy by LIBS. However, more robust detection algorithms are still required to enable samples' quick and accurate classification. A liquid-to-solid phase transformation can significantly boost the trace element concentration, which helps attain a lower LoD and allows for easier identification of trace and hazardous elements by LIBS. For these LIBS-linked approaches, a major challenge is maintaining reproducibility and repeatability for trace element quantification, and more in-depth research needs to be carried out in the future.

Data Availability

No data were used in this study.

Conflicts of Interest

The authors declare that they have no conflicts of interest regarding the publication of this article.

References

[1] D. A. Cremers and L. J. Radziemski, *Handbook of Laser-Induced Breakdown Spectroscopy*, John Wiley & Sons, Hoboken, NJ, USA, 2013.

[2] A. W. Miziolek, V. Palleschi, and I. Schechter, *Laser Induced Breakdown Spectroscopy*, Cambridge university press, Cambridge, UK, 2006.

[3] R. Noll, *Laser-induced Breakdown Spectroscopy*, Springer, Berlin, Germany, 2012.

[4] J. P. Singh and S. Thakur, *Laser-induced Breakdown Spectroscopy*, Elsevier, Amsterdam, Netherlands, 2020.

[5] S. Musazzi and U. Perini, *Laser-Induced Breakdown Spectroscopy: Theory and Applications*, Springer, Berlin, Germany, 2014.

[6] H. Loudyi, K. Rifaï, S. Laville, F. Vidal, M. Chaker, and M. Sabsabi, "Improving laser-induced breakdown spectroscopy (LIBS) performance for iron and lead determination in aqueous solutions with laser-induced fluorescence (LIF)," *Journal of Analytical Atomic Spectrometry*, vol. 24, pp. 1421–1428, 2009.

[7] A. De Giacomo, C. Koral, G. Valenza, R. Gaudiuso, and M. Dell'Aglio, "Nanoparticle enhanced laser-induced breakdown spectroscopy for microdrop analysis at subppm level," *Analytical Chemistry*, vol. 88, pp. 5251–5257, 2016.

[8] A. Haider, M. Rony, and K. Abedin, "Determination of the ash content of coal without ashing: a simple technique using laser-induced breakdown spectroscopy," *Energy and Fuels*, vol. 27, pp. 3725–3729, 2013.

[9] A. Haider, M. K. Ira, Z. Khan, and K. Abedin, "Radiative lifetime measurement of excited neutral nitrogen atoms by time resolved laser-induced breakdown spectroscopy," *Journal of Analytical Atomic Spectrometry*, vol. 29, pp. 1385–1392, 2014.

[10] M. Sadat, A. Haider, K. Abedin, and M. Wahadoszamen, "Semiquantitative determination of chromium content of river bed soil of buriganga river at different locations," *Journal of Bangladesh Academy of Sciences*, vol. 34, pp. 123–131, 2010.

[11] M. Ahmed, K. Abedin, M. Sadat, A. Talukder, M. Wahadoszamen, and A. Haider, "Elemental profiling of surface water around dhaka city by laser induced breakdown spectroscopy," *Journal of Bangladesh Academy of Sciences*, vol. 33, pp. 209–218, 2009.

[12] F. Tasneem, Z. H. Khan, A. Islam et al., "A rapid method of identification of garnet in beach sands using laser-induced breakdown spectroscopy," *Journal of Bangladesh Academy of Sciences*, vol. 43, pp. 149–157, 2019.

[13] A. Haider, S. Sengupta, and K. Abedin, "A quick method to determine the impurity content in gold ornaments by LIBS technique," in *Proceedings of the 2015 International*

Conference on Photonics, Optics and Laser Technology (PHOTOPTICS), pp. 33–40, Article ID 2015.

[14] F. J. Fortes, J. Moros, P. Lucena, L. M. Cabalín, and J. J. Laserna, "Laser-induced breakdown spectroscopy," *Analytical Chemistry*, vol. 85, pp. 640–669, 2012.

[15] A. Haider, M. H. Ullah, Z. H. Khan, F. Kabir, and K. M. Abedin, "Detection of trace amount of arsenic in groundwater by laser-induced breakdown spectroscopy and adsorption," *Optics & Laser Technology*, vol. 56, pp. 299–303, 2014.

[16] D. N. Stratis, K. L. Eland, and S. M. Angel, "Dual-pulse LIBS using a pre-ablation spark for enhanced ablation and emission," *Applied Spectroscopy*, vol. 54, pp. 1270–1274, 2000.

[17] R. Noll, R. Sattmann, V. Sturm, and S. Winkelmann, "Space- and time-resolved dynamics of plasmas generated by laser double pulses interacting with metallic samples," *Journal of Analytical Atomic Spectrometry*, vol. 19, pp. 419–428, 2004.

[18] G. Cristoforetti, S. Legnaioli, V. Palleschi, A. Salvetti, and E. Tognoni, "Characterization of a collinear double pulse laser-induced plasma at several ambient gas pressures by spectrally-and time-resolved imaging," *Applied Physics B*, vol. 80, pp. 559–568, 2005.

[19] J. Scaffidi, W. Pearman, J. Carter, and S. Angel, "Observations in collinear femtosecond—nanosecond dual-pulse laser-induced breakdown spectroscopy," *Applied Spectroscopy*, vol. 60, pp. 65–71, 2006.

[20] B. Rashid, R. Ahmed, R. Ali, and M. Baig, "A comparative study of single and double pulse of laser induced breakdown spectroscopy of silver," *Physics of Plasmas*, vol. 18, Article ID 073301, 2011.

[21] C. R. Bhatt, D. Hartzler, J. C. Jain, and D. L. McIntyre, "Evaluation of analytical performance of double pulse laser-induced breakdown spectroscopy for the detection of rare earth elements," *Optics & Laser Technology*, vol. 126, Article ID 106110, 2020.

[22] A. Kuwako, Y. Uchida, and K. Maeda, "Supersensitive detection of sodium in water with use of dual-pulse laser-induced breakdown spectroscopy," *Applied Optics*, vol. 42, pp. 6052–6056, 2003.

[23] J. Uebbing, J. Brust, W. Sdorra, F. Leis, and K. Niemax, "Reheating of a laser-produced plasma by a second pulse laser," *Applied Spectroscopy*, vol. 45, pp. 1419–1423, 1991.

[24] J. Scaffidi, S. M. Angel, and D. A. Cremers, *Emission Enhancement Mechanisms in Dual-Pulse LIBS*ACS Publications, Washington, DC, USA, 2006.

[25] S. M. Angel, D. N. Stratis, K. L. Eland, T. Lai, M. A. Berg, and D. M. Gold, "LIBS using dual-and ultra-short laser pulses," *Fresenius' Journal of Analytical Chemistry'*, vol. 369, pp. 320–327, 2001.

[26] F. C. De Lucia, J. L. Gottfried, and A. W. Miziolek, "Evaluation of femtosecond laser-induced breakdown spectroscopy for explosive residue detection," *Optics Express*, vol. 17, pp. 419–425, 2009.

[27] A. Elhassan, A. Giakoumaki, D. Anglos, G. Ingo, L. Robbiola, and M. Harith, "Nanosecond and femtosecond laser induced breakdown spectroscopic analysis of bronze alloys," *Spectrochimica Acta Part B: Atomic Spectroscopy*, vol. 63, pp. 504–511, 2008.

[28] J. Freeman, S. Harilal, P. Diwakar, B. Verhoff, and A. Hassanein, "Comparison of optical emission from nanosecond and femtosecond laser produced plasma in atmosphere and vacuum conditions," *Spectrochimica Acta Part B: Atomic Spectroscopy*, vol. 87, pp. 43–50, 2013.

[29] S. Harilal, J. Freeman, P. Diwakar, and A. Hassanein, "Comparison of nanosecond and femtosecond LIBS," in *Proceedings of the CLEO: Science and Innovations, Optical Society of America*, San Jose, CA, USA, 2013.

[30] K. Al-Shboul, S. Harilal, and A. Hassanein, "Spatio-temporal mapping of ablated species in ultrafast laser-produced graphite plasmas," *Applied Physics Letters*, vol. 100, Article ID 221106, 2012.

[31] S. Tzortzakis, D. Gray, and D. Anglos, "Femtosecond laser filaments enable remote LIBS analysis with potential applications in the monitoring of sculpture and monuments," *Optics Letters*, vol. 31, pp. 1139–1141, 2006.

[32] R. Grönlund, M. Lundqvist, and S. Svanberg, "Remote imaging laser-induced breakdown spectroscopy and remote cultural heritage ablative cleaning," *Optics Letters*, vol. 30, pp. 2882–2884, 2005.

[33] V. S. Dhanada, S. D. George, V. Kartha, S. Chidangil, and V. K. Unnikrishnan, "Hybrid LIBS-raman-LIF systems for multi-modal spectroscopic applications: a topical review," *Applied Spectroscopy Reviews*, vol. 56, pp. 1–29, 2020.

[34] K. J. Mason and J. M. Goldberg, "Characterization of a laser plasma in a pulsed magnetic field. part I: spatially resolved emission studies," *Applied Spectroscopy*, vol. 45, pp. 370–379, 1991.

[35] V. N. Rai, H. Zhang, F. Y. Yueh, J. P. Singh, and A. Kumar, "Effect of steady magnetic field on laser-induced breakdown spectroscopy," *Applied Optics*, vol. 42, pp. 3662–3669, 2003.

[36] D. Fried, G. P. Reck, T. Kushida, and E. Rothe, "Electric field enhancement of optical emission from plasma plume generated during ArF excimer photoablation of BaO_2, Y_2O_3, CuO and $YBa_2Cu_3O_7$," *Journal of Physics D: Applied Physics*, vol. 24, p. 1065, 1991.

[37] F. O. Bredice, D. O. Orzi, D. Schinca, H. Sobral, and M. Villagran-Muniz, "Characterization of pulsed laser generated plasma through its perturbation in an electric field," *IEEE Transactions on Plasma Science*, vol. 30, pp. 2139–2143, 2002.

[38] O. A. Nassef and H. E. Elsayed-Ali, "Spark discharge assisted laser induced breakdown spectroscopy," *Spectrochimica Acta Part B: Atomic Spectroscopy*, vol. 60, pp. 1564–1572, 2005.

[39] L. Kexue, W. Zhou, Q. Shen, J. Shao, and H. Qian, "Signal enhancement of lead and arsenic in soil using laser ablation combined with fast electric discharge," *Spectrochimica Acta Part B: Atomic Spectroscopy*, vol. 65, pp. 420–424, 2010.

[40] F. F. Chen, *Introduction to Plasma Physics and Controlled Fusion*, Springer, Berlin, Germany, 1984.

[41] Y. Liu, M. Baudelet, and M. Richardson, "Elemental analysis by microwave-assisted laser-induced breakdown spectroscopy: evaluation on ceramics," *Journal of Analytical Atomic Spectrometry*, vol. 25, pp. 1316–1323, 2010.

[42] A. A. Al Shuaili, A. M. Al Hadhrami, M. A. Wakil, and Z. T. Alwahabi, "Improvement of palladium limit of detection by microwave-assisted laser induced breakdown spectroscopy," *Spectrochimica Acta Part B: Atomic Spectroscopy*, vol. 159, Article ID 105666, 2019.

[43] C. Goueguel, S. Laville, F. Vidal, M. Chaker, and M. Sabsabi, "Resonant laser-induced breakdown spectroscopy for analysis of lead traces in copper alloys," *Journal of Analytical Atomic Spectrometry*, vol. 26, pp. 2452–2460, 2011.

[44] C. Goueguel, S. Laville, F. Vidal, M. Sabsabi, and M. Chaker, "Investigation of resonance-enhanced laser-induced breakdown spectroscopy for analysis of aluminium alloys," *Journal of Analytical Atomic Spectrometry*, vol. 25, pp. 635–644, 2010.

[45] K. Rifai, F. Vidal, M. Chaker, and M. Sabsabi, "Resonant laser-induced breakdown spectroscopy (RLIBS) analysis of traces through selective excitation of aluminum in aluminum alloys," *Journal of Analytical Atomic Spectrometry*, vol. 28, pp. 388–395, 2013.

[46] K. Muhammed Shameem, V. Dhanada, V. Unnikrishnan, S. D. George, V. Kartha, and C. Santhosh, "A hyphenated echelle LIBS-raman system for multi-purpose applications," *Review of Scientific Instruments*, vol. 89, Article ID 073108, 2018.

[47] K. M. Shameem, K. S. Choudhari, A. Bankapur et al., "A hybrid LIBS–raman system combined with chemometrics: an efficient tool for plastic identification and sorting," *Analytical and Bioanalytical Chemistry*, vol. 409, pp. 3299–3308, 2017.

[48] M. Hoehse, A. Paul, I. Gornushkin, and U. Panne, "Multivariate classification of pigments and inks using combined raman spectroscopy and LIBS," *Analytical and Bioanalytical Chemistry*, vol. 402, pp. 1443–1450, 2012.

[49] G. B. Courreges-Lacoste, B. Ahlers, and F. R. Perez, "Combined raman spectrometer/laser-induced breakdown spectrometer for the next ESA mission to mars," *Spectrochimica Acta Part A: Molecular and Biomolecular Spectroscopy*, vol. 68, pp. 1023–1028, 2007.

[50] K. Muhammed Shameem, A. Chawla, M. Mallya et al., "Laser-induced breakdown spectroscopy-raman: an effective complementary approach to analyze renal-calculi," *Journal of Biophotonics*, vol. 11, Article ID e201700271, 2018.

[51] Q. Lin, G. Niu, Q. Wang, Q. Yu, and Y. Duan, "Combined laser-induced breakdown with raman spectroscopy: historical technology development and recent applications," *Applied Spectroscopy Reviews*, vol. 48, pp. 487–508, 2013.

[52] S. A. Maier, *Plasmonics: Fundamentals and Applications*, Springer Science & Business Media, Berlin, Germany, 2007.

[53] M. Dell'Aglio, R. Alrifai, and A. De Giacomo, "Nanoparticle enhanced laser induced breakdown spectroscopy (NELIBS), a first review," *Spectrochimica Acta Part B: Atomic Spectroscopy*, vol. 148, pp. 105–112, 2018.

[54] F. Schertz, M. Schmelzeisen, M. Kreiter, H.-J. Elmers, and G. Schönhense, "Field emission of electrons generated by the near field of strongly coupled plasmons," *Physical Review Letters*, vol. 108, Article ID 237602, 2012.

[55] A. De Giacomo, M. Dell'Aglio, R. Gaudiuso, C. Koral, and G. Valenza, "Perspective on the use of nanoparticles to improve LIBS analytical performance: nanoparticle enhanced laser induced breakdown spectroscopy (NELIBS)," *Journal of Analytical Atomic Spectrometry*, vol. 31, pp. 1566–1573, 2016.

[56] V. Rai and S. N. Thakur, "Instrumentation for LIBS and recent advances," in *Laser-Induced Breakdown Spectroscopy*, pp. 107–136, Elsevier, Amsterdam, Netherlands, 2020.

[57] D. F. Andrade and E. R. Pereira-Filho, "Direct determination of contaminants and major and minor nutrients in solid fertilizers using laser-induced breakdown spectroscopy (LIBS)," *Journal of Agricultural and Food Chemistry*, vol. 64, pp. 7890–7898, 2016.

[58] R. Lasheras, C. Bello-Gálvez, and J. Anzano, "Quantitative analysis of oxide materials by laser-induced breakdown spectroscopy with argon as an internal standard," *Spectrochimica Acta Part B: Atomic Spectroscopy*, vol. 82, pp. 65–70, 2013.

[59] L. Sheng, T. Zhang, K. Wang, H. Tang, and H. Li, "Quantitative analysis of Fe content in iron ore via external calibration in conjunction with internal standardization method coupled with LIBS," *Chemical Research in Chinese Universities*, vol. 31, pp. 107–111, 2015.

[60] H. Fu, J. Jia, H. Wang, Z. Ni, and F. Dong, "Calibration methods of laser-induced breakdown spectroscopy," in *Calibration and Validation of Analytical Methods-A Sampling of Current Approaches*IntechOpen, London, UK, 2017.

[61] M. Dong, D. Oropeza, J. Chirinos et al., "Elemental analysis of coal by tandem laser induced breakdown spectroscopy and laser ablation inductively coupled plasma time of flight mass spectrometry," *Spectrochimica Acta Part B: Atomic Spectroscopy*, vol. 109, pp. 44–50, 2015.

[62] F. Rezaei, P. Karimi, and S. Tavassoli, "Effect of self-absorption correction on LIBS measurements by calibration curve and artificial neural network," *Applied Physics B*, vol. 114, pp. 591–600, 2014.

[63] L. Sheng, T. Zhang, G. Niu et al., "Classification of iron ores by laser-induced breakdown spectroscopy (LIBS) combined with random forest (RF)," *Journal of Analytical Atomic Spectrometry*, vol. 30, pp. 453–458, 2015.

[64] J. Yang, C. Yi, J. Xu, and X. Ma, "Laser-induced breakdown spectroscopy quantitative analysis method via adaptive analytical line selection and relevance vector machine regression model," *Spectrochimica Acta Part B: Atomic Spectroscopy*, vol. 107, pp. 45–55, 2015.

[65] Y. Wu, J. Ouyang, and T. Sun, "Quantitative analysis of lead in soybean oil by double pulse laser-induced breakdown spectroscopy and multivariate calibration method," *Journal of Instrumental Analysis*, vol. 35, pp. 1015–1020, 2016.

[66] M. Dyar, M. Carmosino, E. Breves, M. Ozanne, S. Clegg, and R. Wiens, "Comparison of partial least squares and lasso regression techniques as applied to laser-induced breakdown spectroscopy of geological samples," *Spectrochimica Acta Part B: Atomic Spectroscopy*, vol. 70, pp. 51–67, 2012.

[67] M. Aguirre, E. Selva, M. Hidalgo, and A. Canals, "Dispersive liquid–liquid microextraction for metals enrichment: a useful strategy for improving sensitivity of laser-induced breakdown spectroscopy in liquid samples analysis," *Talanta*, vol. 131, pp. 348–353, 2015.

[68] A. Matsumoto, A. Tamura, R. Koda et al., "On-site quantitative elemental analysis of metal ions in aqueous solutions by underwater laser-induced breakdown spectroscopy combined with electrodeposition under controlled potential," *Analytical Chemistry*, vol. 87, pp. 1655–1661, 2015.

[69] X. Wang, Y. Wei, Q. Lin, J. Zhang, and Y. Duan, "Simple, fast matrix conversion and membrane separation method for ultrasensitive metal detection in aqueous samples by laser-induced breakdown spectroscopy," *Analytical Chemistry*, vol. 87, pp. 5577–5583, 2015.

[70] Z. Chen, H. Li, M. Liu, and R. Li, "Fast and sensitive trace metal analysis in aqueous solutions by laser-induced breakdown spectroscopy using wood slice substrates," *Spectrochimica Acta Part B: Atomic Spectroscopy*, vol. 63, pp. 64–68, 2008.

[71] D. Zhu, J. Chen, J. Lu, and X. Ni, "Laser-induced breakdown spectroscopy for determination of trace metals in aqueous solution using bamboo charcoal as a solid-phase extraction adsorbent," *Analytical Methods*, vol. 4, pp. 819–823, 2012.

[72] R. L. Vander Wal, T. M. Ticich, J. R. West, and P. A. Householder, "Trace metal detection by laser-induced breakdown spectroscopy," *Applied Spectroscopy*, vol. 53, pp. 1226–1236, 1999.

[73] A. Haider, M. Parvin, Z. Khan, and M. Wahadoszamen, "Highly sensitive detection of lead in aqueous solution using laser-induced breakdown spectroscopy coupled with

adsorption technique," *Journal of Applied Spectroscopy*, vol. 87, pp. 1163–1170, 2021.

[74] Q. Lin, Z. Wei, M. Xu et al., "Laser-induced breakdown spectroscopy for solution sample analysis using porous electrospun ultrafine fibers as a solid-phase support," *RSC Advances*, vol. 4, pp. 14392–14399, 2014.

[75] Z. Chen, H. Li, F. Zhao, and R. Li, "Ultra-sensitive trace metal analysis of water by laser-induced breakdown spectroscopy after electrical-deposition of the analytes on an aluminium surface," *Journal of Analytical Atomic Spectrometry*, vol. 23, pp. 871–875, 2008.

[76] D. D. Pace, C. D'Angelo, D. Bertuccelli, and G. Bertuccelli, "Analysis of heavy metals in liquids using laser induced breakdown spectroscopy by liquid-to-solid matrix conversion," *Spectrochimica Acta Part B: Atomic Spectroscopy*, vol. 61, pp. 929–933, 2006.

[77] M. Aguirre, S. Legnaioli, F. Almodóvar, M. Hidalgo, V. Palleschi, and A. Canals, "Elemental analysis by surface-enhanced laser-induced breakdown spectroscopy combined with liquid–liquid microextraction," *Spectrochimica Acta Part B: Atomic Spectroscopy*, vol. 79, pp. 88–93, 2013.

[78] S. Ma, Y. Tang, Y. Ma et al., "Determination of trace heavy metal elements in aqueous solution using surface-enhanced laser-induced breakdown spectroscopy," *Optics Express*, vol. 27, pp. 15091–15099, 2019.

[79] J.-S. Xiu, X.-S. Bai, V. Motto-Ros, and J. Yu, "Characteristics of indirect laser-induced plasma from a thin film of oil on a metallic substrate," *Frontiers of Physics*, vol. 10, pp. 231–239, 2015.

[80] X. Yang, Z. Hao, C. Li et al., "Sensitive determinations of Cu, Pb, Cd, and Cr elements in aqueous solutions using chemical replacement combined with surface-enhanced laser-induced breakdown spectroscopy," *Optics Express*, vol. 24, pp. 13410–13417, 2016.

[81] X. Yang, Z. Hao, R. Yi et al., "Simultaneous determination of La, Ce, Pr, and Nd elements in aqueous solution using surface-enhanced laser-induced breakdown spectroscopy," *Talanta*, vol. 163, pp. 127–131, 2017.

[82] V. Babushok, F. DeLucia, J. Gottfried, C. Munson, and A. Miziolek, "Double pulse laser ablation and plasma: laser induced breakdown spectroscopy signal enhancement," *Spectrochimica Acta Part B: Atomic Spectroscopy*, vol. 61, pp. 999–1014, 2006.

[83] F. Yang, L. Jiang, S. Wang et al., "Emission enhancement of femtosecond laser-induced breakdown spectroscopy by combining nanoparticle and dual-pulse on crystal SiO_2," *Optics & Laser Technology*, vol. 93, pp. 194–200, 2017.

[84] D. Dong, L. Jiao, X. Du, and C. Zhao, "Ultrasensitive nanoparticle enhanced laser-induced breakdown spectroscopy using a super-hydrophobic substrate coupled with magnetic confinement," *Chemical Communications*, vol. 53, pp. 4546–4549, 2017.

[85] M. Wakil and Z. T. Alwahabi, "Microwave-assisted laser induced breakdown molecular spectroscopy: quantitative chlorine detection," *Journal of Analytical Atomic Spectrometry*, vol. 34, pp. 1892–1899, 2019.

[86] X. Fu, G. Li, and D. Dong, "Improving the detection sensitivity for laser-induced breakdown spectroscopy: a review," *Frontiers in Physics*, vol. 8, p. 68, 2020.

[87] T. Wada and W. Hagel, "Effect of trace elements, molybdenum, and intercritical heat treatment on temper embrittlement of 2-1/4Cr-1 Mo steel," *Metallurgical Transactions A*, vol. 7, pp. 1419–1426, 1976.

[88] R. Swindeman, V. Sikka, and R. Klueh, "Residual and trace element effects on the high-temperature creep strength of austenitic stainless steels," *Metallurgical Transactions A*, vol. 14, pp. 581–593, 1983.

[89] D. Melford, "The influence of residual and trace elements on hot shortness and high temperature embrittlement," *Philosophical Transactions of the Royal Society of London—Series A: Mathematical and Physical Sciences*, vol. 295, pp. 89–103, 1980.

[90] X. Jiang, P. Hayden, J. Costello, and E. Kennedy, "Double-pulse laser induced breakdown spectroscopy with ambient gas in the vacuum ultraviolet: optimization of parameters for detection of carbon and sulfur in steel," *Spectrochimica Acta Part B: Atomic Spectroscopy*, vol. 101, pp. 106–113, 2014.

[91] M. Cui, Y. Deguchi, Z. Wang, S. Tanaka, Y. Fujita, and S. Zhao, "Improved analysis of manganese in steel samples using collinear long–short double pulse laser-induced breakdown spectroscopy (LIBS)," *Applied Spectroscopy*, vol. 73, pp. 152–162, 2019.

[92] M. Cui, Y. Deguchi, C. Yao, Z. Wang, S. Tanaka, and D. Zhang, "Carbon detection in solid and liquid steel samples using ultraviolet long-short double pulse laser-induced breakdown spectroscopy," *Spectrochimica Acta Part B: Atomic Spectroscopy*, vol. 167, Article ID 105839, 2020.

[93] M. A. Ismail, G. Cristoforetti, S. Legnaioli et al., "Comparison of detection limits, for two metallic matrices, of laser-induced breakdown spectroscopy in the single and double-pulse configurations," *Analytical and Bioanalytical Chemistry*, vol. 385, pp. 316–325, 2006.

[94] D. Sun, Y. Ma, Y. Wang, M. Su, Q. Lu, and C. Dong, "Determination of the limits of detection for aluminum-based alloys by spatially resolved single-and double-pulse laser-induced breakdown spectroscopy," *Analytical Methods*, vol. 10, pp. 2595–2603, 2018.

[95] R. Hai, L. Sun, D. Wu et al., "Enhanced laser-induced breakdown spectroscopy using the combination of circular and annular laser pulses," *Journal of Analytical Atomic Spectrometry*, vol. 34, pp. 1982–1987, 2019.

[96] A. Santagata, D. Spera, G. Albano et al., "Orthogonal fs/ns double-pulse libs for copper-based-alloy analysis," *Applied Physics A*, vol. 93, pp. 929–934, 2008.

[97] S. A. Abbasi, Z. Aziz, T. M. Khan et al., "Enhancement of optical signal and characterization of palladium plasma by magnetic field-assisted laser-induced breakdown spectroscopy," *Optik*, vol. 224, Article ID 165746, 2020.

[98] Z. Hao, L. Guo, C. Li et al., "Sensitivity improvement in the detection of V and Mn elements in steel using laser-induced breakdown spectroscopy with ring-magnet confinement," *Journal of Analytical Atomic Spectrometry*, vol. 29, pp. 2309–2314, 2014.

[99] X. Shen, H. Wang, Z. Xie, Y. Gao, H. Ling, and Y. Lu, "Detection of trace phosphorus in steel using laser-induced breakdown spectroscopy combined with laser-induced fluorescence," *Applied Optics*, vol. 48, pp. 2551–2558, 2009.

[100] C. Li, Z. Hao, Z. Zou et al., "Determinations of trace boron in superalloys and steels using laser-induced breakdown spectroscopy assisted with laser-induced fluorescence," *Optics Express*, vol. 24, pp. 7850–7857, 2016.

[101] J. Li, L. Guo, N. Zhao et al., "Determination of cobalt in low-alloy steels using laser-induced breakdown spectroscopy combined with laser-induced fluorescence," *Talanta*, vol. 151, pp. 234–238, 2016.

[102] A. A. Khedr, M. A. Sliem, and M. Abdel-Harith, "Gold nanoparticle-enhanced laser-induced breakdown

spectroscopy and three-dimensional contour imaging of an aluminum alloy," *Applied Spectroscopy*, vol. 75, pp. 565–573, 2021.

[103] Y. Jiang, R. Li, and Y. Chen, "Elemental analysis of copper alloys with laser-ablation spark-induced breakdown spectroscopy based on a fiber laser operated at 30 kHz pulse repetition rate," *Journal of Analytical Atomic Spectrometry*, vol. 34, pp. 1838–1845, 2019.

[104] J. Kang, Y. Jiang, R. Li, and Y. Chen, "Sensitive elemental analysis with high repetition rate laser-ablation spark-induced breakdown spectroscopy combined with lock-in signal detection," *Spectrochimica Acta Part B: Atomic Spectroscopy*, vol. 155, pp. 50–55, 2019.

[105] A. Sarkar, V. Karki, S. K. Aggarwal et al., "Evaluation of the prediction precision capability of partial least squares regression approach for analysis of high alloy steel by laser induced breakdown spectroscopy," *Spectrochimica Acta Part B: Atomic Spectroscopy*, vol. 108, pp. 8–14, 2015.

[106] L. Sun, H. Yu, Z. Cong, Y. Xin, Y. Li, and L. Qi, "In situ analysis of steel melt by double-pulse laser-induced breakdown spectroscopy with a cassegrain telescope," *Spectrochimica Acta Part B: Atomic Spectroscopy*, vol. 112, pp. 40–48, 2015.

[107] M. S. Afgan, Z. Hou, and Z. Wang, "Quantitative analysis of common elements in steel using a handheld μ-LIBS instrument," *Journal of Analytical Atomic Spectrometry*, vol. 32, pp. 1905–1915, 2017.

[108] J. He, C. Pan, Y. Liu, and X. Du, "Quantitative analysis of carbon with laser-induced breakdown spectroscopy (libs) using genetic algorithm and back propagation neural network models," *Applied Spectroscopy*, vol. 73, pp. 678–686, 2019.

[109] Y. Zhang, C. Sun, L. Gao et al., "Determination of minor metal elements in steel using laser-induced breakdown spectroscopy combined with machine learning algorithms," *Spectrochimica Acta Part B: Atomic Spectroscopy*, vol. 166, Article ID 105802, 2020.

[110] J. Aguilera, C. Aragon, and J. Campos, "Determination of carbon content in steel using laser-induced breakdown spectroscopy," *Applied Spectroscopy*, vol. 46, pp. 1382–1387, 1992.

[111] V. Sturm, L. Peter, and R. Noll, "Steel analysis with laser-induced breakdown spectrometry in the vacuum ultraviolet," *Applied Spectroscopy*, vol. 54, pp. 1275–1278, 2000.

[112] L. Peter, V. Sturm, and R. Noll, "Liquid steel analysis with laser-induced breakdown spectrometry in the vacuum ultraviolet," *Applied Optics*, vol. 42, pp. 6199–6204, 2003.

[113] M. Hemmerlin, R. Meilland, H. Falk, P. Wintjens, and L. Paulard, "Application of vacuum ultraviolet laser-induced breakdown spectrometry for steel analysis—comparison with spark-optical emission spectrometry figures of merit," *Spectrochimica Acta Part B: Atomic Spectroscopy*, vol. 56, pp. 661–669, 2001.

[114] J. Li, Z. Zhu, R. Zhou et al., "Determination of carbon content in steels using laser-induced breakdown spectroscopy assisted with laser-induced radical fluorescence," *Analytical Chemistry*, vol. 89, pp. 8134–8139, 2017.

[115] A. Gonzcález, M. Ortiz, and J. Campos, "Determination of sulfur content in steel by laser-produced plasma atomic emission spectroscopy," *Applied Spectroscopy*, vol. 49, pp. 1632–1635, 1995.

[116] N. Ahmed, R. Ahmed, and M. A. Baig, "Analytical analysis of different karats of gold using laser induced breakdown spectroscopy (LIBS) and laser ablation time of flight mass spectrometer (LA-TOF-MS)," *Plasma Chemistry and Plasma Processing*, vol. 38, pp. 207–222, 2018.

[117] J. Kaiser, K. Novotný, M. Z. Martin et al., "Trace elemental analysis by laser-induced breakdown spectroscopy—biological applications," *Surface Science Reports*, vol. 67, pp. 233–243, 2012.

[118] M. Yao, H. Yang, L. Huang, T. Chen, G. Rao, and M. Liu, "Detection of heavy metal Cd in polluted fresh leafy vegetables by laser-induced breakdown spectroscopy," *Applied Optics*, vol. 56, pp. 4070–4075, 2017.

[119] A. F. Haider, F. Kabir, M. H. Ullah, Z. Khan, and K. M. Abedin, "Elemental profiling and identification of ecotoxic elements in agricultural soil by laser-induced breakdown spectroscopy," *Applied Ecology and Environmental Sciences*, vol. 1, pp. 41–44, 2013.

[120] G. Kim, J. Kwak, J. Choi, and K. Park, "Detection of nutrient elements and contamination by pesticides in spinach and rice samples using laser-induced breakdown spectroscopy (LIBS)," *Journal of Agricultural and Food Chemistry*, vol. 60, pp. 718–724, 2012.

[121] Z. Luo, H. Rao, L. Huang et al., "Effect of Cu stress on minerals in rice by analyzing husk based on laser-induced breakdown spectroscopy," *Applied Physics B*, vol. 126, pp. 1–9, 2020.

[122] M. Pérez-Rodríguez, P. M. Dirchwolf, T. V. Silva et al., "Fast spark discharge-laser-induced breakdown spectroscopy method for rice botanic origin determination," *Food Chemistry*, vol. 331, Article ID 127051, 2020.

[123] M. G. Nespeca, A. L. Vieira, D. S. Júnior, J. A. G. Neto, and E. C. Ferreira, "Detection and quantification of adulterants in honey by LIBS," *Food Chemistry*, vol. 311, Article ID 125886, 2020.

[124] B. Sezer, A. Bjelak, H. M. Velioglu, and I. H. Boyaci, "Protein based evaluation of meat species by using laser induced breakdown spectroscopy," *Meat Science*, vol. 172, Article ID 108361, 2021.

[125] L. Guo, W. Zheng, F. Chen et al., "Meat species identification accuracy improvement using sample set portioning based on joint x-y distance and laser-induced breakdown spectroscopy," *Applied Optics*, vol. 60, pp. 5826–5831, 2021.

[126] M. Zhao, M. Markiewicz-Keszycka, R. J. Beattie et al., "Quantification of calcium in infant formula using laser-induced breakdown spectroscopy (LIBS), fourier transform mid-infrared (FT-IR) and raman spectroscopy combined with chemometrics including data fusion," *Food Chemistry*, vol. 320, Article ID 126639, 2020.

[127] W. Wang, W. Kong, T. Shen et al., "Quantitative analysis of cadmium in rice roots based on LIBS and chemometrics methods," *Environmental Sciences Europe*, vol. 33, pp. 1–14, 2021.

[128] Y. Tian, Q. Chen, Y. Lin, Y. Lu, Y. Li, and H. Lin, "Quantitative determination of phosphorus in seafood using laser-induced breakdown spectroscopy combined with machine learning," *Spectrochimica Acta Part B: Atomic Spectroscopy*, vol. 175, Article ID 106027, 2021.

[129] P. A. Akın, B. Sezer, S. R. Bean et al., "Analysis of corn and sorghum flour mixtures using laser-induced breakdown spectroscopy," *Journal of the Science of Food and Agriculture*, vol. 101, pp. 1076–1084, 2021.

[130] A. Mehder, Y. Habibullah, M. Gondal, and U. Baig, "Qualitative and quantitative spectro-chemical analysis of dates using UV-pulsed laser induced breakdown spectroscopy and inductively coupled plasma mass spectrometry," *Talanta*, vol. 155, pp. 124–132, 2016.

[131] B. Sezer, G. Bilge, A. Berkkan, U. Tamer, and I. H. Boyaci, "A rapid tool for determination of titanium dioxide content in white chickpea samples," *Food Chemistry*, vol. 240, pp. 84–89, 2018.

[132] V. C. Costa, D. V. de Babos, F. W. B. de Aquino, A. Virgílio, F. A. C. Amorim, and E. R. Pereira-Filho, "Direct determination of Ca, K and Mg in cassava flour samples by laser-induced breakdown spectroscopy (LIBS)," *Food Analytical Methods*, vol. 11, pp. 1886–1896, 2018.

[133] M. Gondal, Y. Habibullah, U. Baig, and L. Oloore, "Direct spectral analysis of tea samples using 266 nm UV pulsed laser-induced breakdown spectroscopy and cross validation of LIBS results with ICP-MS," *Talanta*, vol. 152, pp. 341–352, 2016.

[134] L. C. Peruchi, L. C. Nunes, G. G. A. de Carvalho et al., "Determination of inorganic nutrients in wheat flour by laser-induced breakdown spectroscopy and energy dispersive X-ray fluorescence spectrometry," *Spectrochimica Acta Part B: Atomic Spectroscopy*, vol. 100, pp. 129–136, 2014.

[135] X. Zhao, C. Zhao, X. Du, and D. Dong, "Detecting and mapping harmful chemicals in fruit and vegetables using nanoparticle-enhanced laser-induced breakdown spectroscopy," *Scientific Reports*, vol. 9, pp. 1–10, 2019.

[136] J. Singh, R. Kumar, S. Awasthi, V. Singh, and A. Rai, "Laser induced breakdown spectroscopy: a rapid tool for the identification and quantification of minerals in cucurbit seeds," *Food Chemistry*, vol. 221, pp. 1778–1783, 2017.

[137] G. Bilge, İ. H. Boyacı, K. E. Eseller, U. Tamer, and S. Çakır, "Analysis of bakery products by laser-induced breakdown spectroscopy," *Food Chemistry*, vol. 181, pp. 186–190, 2015.

[138] X. Cama-Moncunill, M. Markiewicz-Keszycka, Y. Dixit et al., "Feasibility of laser-induced breakdown spectroscopy (LIBS) as an at-line validation tool for calcium determination in infant formula," *Food Control*, vol. 78, pp. 304–310, 2017.

[139] E. C. Ferreira, E. A. Menezes, W. O. Matos, D. M. Milori, A. R. A. Nogueira, and L. Martin-Neto, "Determination of Ca in breakfast cereals by laser induced breakdown spectroscopy," *Food Control*, vol. 21, pp. 1327–1330, 2010.

[140] R. Hedwig, K. Lahna, R. Idroes et al., "Food analysis employing high energy nanosecond laser and low pressure he ambient gas," *Microchemical Journal*, vol. 147, pp. 356–364, 2019.

[141] A. Jabbar, M. Akhtar, S. Mehmood et al., "On the detection of heavy elements in the euphorbia indica plant using laser-induced breakdown spectroscopy and laser ablation time of flight mass spectrometry," *Journal of Analytical Atomic Spectrometry*, vol. 34, pp. 954–962, 2019.

[142] A. Jabbar, B. Rehman, M. Iqbal, R. Ahmed, S. Mahmood, and M. A. Baig, "Elemental analysis of plants cultivated in saline soil by laser-induced breakdown spectroscopy (LIBS)," *Analytical Letters*, vol. 54, pp. 1351–1365, 2021.

[143] A. Jabbar, M. Akhtar, S. Mehmmod, M. Iqbal, R. Ahmed, and M. Baig, "Quantification of copper remediation in the *Allium cepa* L. leaves using electric field assisted laser induced breakdown spectroscopy," *Spectrochimica Acta Part B: Atomic Spectroscopy*, vol. 162, Article ID 105719, 2019.

[144] O. Samek, J. Lambert, R. Hergenröder et al., "Femtosecond laser spectrochemical analysis of plant samples," *Laser Physics Letters*, vol. 3, p. 21, 2005.

[145] L. Su, W. Shi, X. Chen et al., "Simultaneously and quantitatively analyze the heavy metals in *Sargassum fusiforme* by laser-induced breakdown spectroscopy," *Food Chemistry*, vol. 338, Article ID 127797, 2021.

[146] L. C. Nunes, J. W. B. Braga, L. C. Trevizan et al., "Optimization and validation of a LIBS method for the determination of macro and micronutrients in sugar cane leaves," *Journal of Analytical Atomic Spectrometry*, vol. 25, pp. 1453–1460, 2010.

[147] J. Peng, Y. He, L. Ye et al., "Moisture influence reducing method for heavy metals detection in plant materials using laser-induced breakdown spectroscopy: a case study for chromium content detection in rice leaves," *Analytical Chemistry*, vol. 89, pp. 7593–7600, 2017.

[148] G. G. A. de Carvalho, J. Moros, D. Santos, F. J. Krug, and J. J. Laserna, "Direct determination of the nutrient profile in plant materials by femtosecond laser-induced breakdown spectroscopy," *Analytica Chimica Acta*, vol. 876, pp. 26–38, 2015.

[149] J. W. B. Braga, L. C. Trevizan, L. C. Nunes, I. A. Rufini, D. Santos, and F. J. Krug, "Comparison of univariate and multivariate calibration for the determination of micronutrients in pellets of plant materials by laser induced breakdown spectrometry," *Spectrochimica Acta Part B: Atomic Spectroscopy*, vol. 65, pp. 66–74, 2010.

[150] L. Yang, L. Meng, H. Gao et al., "Building a stable and accurate model for heavy metal detection in mulberry leaves based on a proposed analysis framework and laser-induced breakdown spectroscopy," *Food Chemistry*, vol. 338, Article ID 127886, 2021.

[151] W. Wang, W. Kong, T. Shen et al., "Application of laser-induced breakdown spectroscopy in detection of cadmium content in rice stems," *Frontiers of Plant Science*, vol. 11, p. 2073, 2020.

[152] L. C. Trevizan, D. Santos, R. E. Samad et al., "Evaluation of laser induced breakdown spectroscopy for the determination of micronutrients in plant materials," *Spectrochimica Acta Part B: Atomic Spectroscopy*, vol. 64, pp. 369–377, 2009.

[153] G. G. A. de Carvalho, D. S. Junior, L. C. Nunes, M. da Silva Gomes, F. de Oliveira Leme, and F. J. Krug, "Effects of laser focusing and fluence on the analysis of pellets of plant materials by laser-induced breakdown spectroscopy," *Spectrochimica Acta Part B: Atomic Spectroscopy*, vol. 74, pp. 162–168, 2012.

[154] M. M. El-Deftar, J. Robertson, S. Foster, and C. Lennard, "Evaluation of elemental profiling methods, including laser-induced breakdown spectroscopy (LIBS), for the differentiation of cannabis plant material grown in different nutrient solutions," *Forensic Science International*, vol. 251, pp. 95–106, 2015.

[155] A. M. Roldán, V. Dwivedi, J. Y. S. de los Terreros, and P. Veis, "Laser-Induced breakdown spectroscopy (LIBS) for the analyses of faunal bones: assembling of individuals and elemental quantification," *Optik*, vol. 218, Article ID 164992, 2020.

[156] S. Moncayo, S. Manzoor, T. Ugidos, F. Navarro-Villoslada, and J. Caceres, "Discrimination of human bodies from bones and teeth remains by laser induced breakdown spectroscopy and neural networks," *Spectrochimica Acta Part B: Atomic Spectroscopy*, vol. 101, pp. 21–25, 2014.

[157] P. Siozos, N. Hausmann, M. Holst, and D. Anglos, "Application of laser-induced breakdown spectroscopy and neural networks on archaeological human bones for the discrimination of distinct individuals," *Journal of Archaeological Science: Report*, vol. 35, Article ID 102769, 2021.

[158] G. Gomes, F. Borges, F. Borghi et al., "Rapid stoichiometric analysis of calcium-phosphorus ratio on hydroxyapatite targets by one-point calibration laser-induced breakdown

spectroscopy (OPC-LIBS)," *Spectrochimica Acta Part B: Atomic Spectroscopy*, vol. 184, Article ID 106250, 2021.

[159] M. Martinez and M. Baudelet, "Matrix-matched calibration material for zinc analysis of human nails by laser-induced breakdown spectroscopy," *Spectrochimica Acta Part B: Atomic Spectroscopy*, vol. 163, Article ID 105732, 2020.

[160] O. Samek, H. H. Telle, and D. C. Beddows, "Laser-induced breakdown spectroscopy: a tool for real-time, in vitro and in vivo identification of carious teeth," *BMC Oral Health*, vol. 1, pp. 1–9, 2001.

[161] A. N. Ahmed, M. J. Alwazzan, and M. A. Ismael, "Study effects of pulse laser energy on human primary teeth and extraction caries area by using image processing techniques," *NeuroQuantology*, vol. 18, p. 36, 2020.

[162] S. J. Rehse, J. Diedrich, and S. Palchaudhuri, "Identification and discrimination of *Pseudomonas aeruginosa* bacteria grown in blood and bile by laser-induced breakdown spectroscopy," *Spectrochimica Acta Part B: Atomic Spectroscopy*, vol. 62, pp. 1169–1176, 2007.

[163] A. C. Samuels, F. C. DeLucia, K. L. McNesby, and A. W. Miziolek, "Laser-induced breakdown spectroscopy of bacterial spores, molds, pollens, and protein: initial studies of discrimination potential," *Applied Optics*, vol. 42, pp. 6205–6209, 2003.

[164] M. Dell'Aglio, Z. Salajková, A. Mallardi et al., "Sensing nanoparticle-protein corona using nanoparticle enhanced laser induced breakdown spectroscopy signal enhancement," *Talanta*, vol. 235, Article ID 122741, 2021.

[165] A. Haider and Z. Khan, "Determination of Ca content of coral skeleton by analyte additive method using the LIBS technique," *Optics & Laser Technology*, vol. 44, pp. 1654–1659, 2012.

[166] V. K. Singh, V. Singh, A. K. Rai, S. N. Thakur, P. K. Rai, and J. P. Singh, "Quantitative analysis of gallstones using laser-induced breakdown spectroscopy," *Applied Optics*, vol. 47, pp. G38–G47, 2008.

[167] G. Cristoforetti, M. Corsi, M. Giuffrida et al., "Micro-LIBS and micro-raman spectroscopic analysis of ancient pottery," in *Laser Induced Plasma Spectroscopy and Applications*Optical Society of America, Washington, DC, USA, 2002.

[168] I. Osticioli, N. Mendes, A. Nevin, F. P. Gil, M. Becucci, and E. Castellucci, "Analysis of natural and artificial ultramarine blue pigments using laser induced breakdown and pulsed raman spectroscopy, statistical analysis and light microscopy," *Spectrochimica Acta Part A: Molecular and Biomolecular Spectroscopy*, vol. 73, pp. 525–531, 2009.

[169] V. Lazic, F. Colao, R. Fantoni et al., "Characterisation of lustre and pigment composition in ancient pottery by laser induced fluorescence and breakdown spectroscopy," *Journal of Cultural Heritage*, vol. 4, pp. 303–308, 2003.

[170] Z. E. Papliaka, A. Philippidis, P. Siozos, M. Vakondiou, K. Melessanaki, and D. Anglos, "A multi-technique approach, based on mobile/portable laser instruments, for the in situ pigment characterization of stone sculptures on the island of crete dating from venetian and ottoman period," *Heritage Science*, vol. 4, pp. 1–18, 2016.

[171] D. J. Phares, J. K. Holt, G. T. Smedley, and R. Flagan, "Method for characterization of adhesion properties of trace explosives in fingerprints and fingerprint simulations," *Journal of Forensic Sciences*, vol. 45, pp. 774–784, 2000.

[172] F. C. De Lucia, R. S. Harmon, K. L. McNesby, R. J. Winkel, and A. W. Miziolek, "Laser-induced breakdown spectroscopy analysis of energetic materials," *Applied Optics*, vol. 42, pp. 6148–6152, 2003.

[173] J. L. Gottfried, F. C. De Lucia, C. A. Munson, and A. W. Miziolek, "Laser-induced breakdown spectroscopy for detection of explosives residues: a review of recent advances, challenges, and future prospects," *Analytical and Bioanalytical Chemistry*, vol. 395, pp. 283–300, 2009.

[174] C. Lopez-Moreno, S. Palanco, J. J. Laserna et al., "Test of a stand-off laser-induced breakdown spectroscopy sensor for the detection of explosive residues on solid surfaces," *Journal of Analytical Atomic Spectrometry*, vol. 21, pp. 55–60, 2006.

[175] J. L. Gottfried, F. C. De Lucia, C. A. Munson, and A. W. Miziolek, "Strategies for residue explosives detection using laser-induced breakdown spectroscopy," *Journal of Analytical Atomic Spectrometry*, vol. 23, pp. 205–216, 2008.

[176] J. J. Brady, S. D. Roberson, M. E. Farrell, E. L. Holthoff, D. N. Stratis-Cullum, and P. M. Pellegrino, *Laser-induced Breakdown Spectroscopy: A Review of Applied Explosive Detection*, Army Research Laboratory, Adelphi, MD, USA, 2013.

[177] L. St-Onge, V. Detalle, and M. Sabsabi, "Enhanced laser-induced breakdown spectroscopy using the combination of fourth-harmonic and fundamental Nd: YAG laser pulses," *Spectrochimica Acta Part B: Atomic Spectroscopy*, vol. 57, pp. 121–135, 2002.

[178] J. L. Gottfried, F. C. De Lucia, C. A. Munson, and A. W. Miziolek, "Double-pulse standoff laser-induced breakdown spectroscopy for versatile hazardous materials detection," *Spectrochimica Acta Part B: Atomic Spectroscopy*, vol. 62, pp. 1405–1411, 2007.

[179] C. R. Bhatt, F. Y. Yueh, and J. P. Singh, "Univariate and multivariate analyses of rare earth elements by laser-induced breakdown spectroscopy," *Applied Optics*, vol. 56, pp. 2280–2287, 2017.

[180] J. P. Castro, D. V. Babos, and E. R. Pereira-Filho, "Calibration strategies for the direct determination of rare earth elements in hard disk magnets using laser-induced breakdown spectroscopy," *Talanta*, vol. 208, Article ID 120443, 2020.

[181] G. Hull, H. Lambert, K. Haroon et al., "Quantitative prediction of rare earth concentrations in salt matrices using laser-induced breakdown spectroscopy for application to molten salt reactors and pyroprocessing," *Journal of Analytical Atomic Spectrometry*, vol. 36, pp. 92–102, 2021.

[182] M. Martin, D. Hamm, S. Martin, S. Allman, G. Bell, and R. Martin, "Micro-laser-induced breakdown spectroscopy: a novel approach used in the detection of six rare earths and one transition metal," *Minerals*, vol. 9, p. 103, 2019.

[183] M. Tampo, M. Miyabe, K. Akaoka et al., "Enhancement of intensity in microwave-assisted laser-induced breakdown spectroscopy for remote analysis of nuclear fuel recycling," *Journal of Analytical Atomic Spectrometry*, vol. 29, pp. 886–892, 2014.

[184] K. Abedin, A. Haider, M. Rony, and Z. Khan, "Identification of multiple rare earths and associated elements in raw monazite sands by laser-induced breakdown spectroscopy," *Optics & Laser Technology*, vol. 43, pp. 45–49, 2011.

[185] A. Haider and Z. H. Khan, "Identification of multiple rare earths and other associated elements in zircon by laser-induced breakdown spectroscopy," *Journal of Bangladesh Academy of Sciences*, vol. 44, 2020.

[186] A. Haider, M. Rony, R. Lubna, and K. Abedin, "Detection of multiple elements in coal samples from Bangladesh by laser-induced breakdown spectroscopy," *Optics & Laser Technology*, vol. 43, pp. 1405–1410, 2011.

[187] C. R. Bhatt, J. C. Jain, C. L. Goueguel, D. L. McIntyre, and J. P. Singh, "Determination of rare earth elements in geological samples using laser-induced breakdown spectroscopy (LIBS)," *Applied Spectroscopy*, vol. 72, pp. 114–121, 2018.

[188] S. Müller, J. A. Meima, and D. Rammlmair, "Detecting REE-rich areas in heterogeneous drill cores from storkwitz using LIBS and a combination of k-means clustering and spatial raster analysis," *Journal of Geochemical Exploration*, vol. 221, Article ID 106697, 2021.

[189] X. Shen and Y. Lu, "Detection of uranium in solids by using laser-induced breakdown spectroscopy combined with laser-induced fluorescence," *Applied Optics*, vol. 47, pp. 1810–1815, 2008.

[190] Y. Youli, Z. Weidong, Q. Huiguo, S. Xuejiao, and R. Ke, "Simultaneous determination of trace lead and chromium in water using laser-induced breakdown spectroscopy and paper substrate," *Plasma Science and Technology*, vol. 16, p. 683, 2014.

[191] H. Tian, L. Jiao, and D. Dong, "Rapid determination of trace cadmium in drinking water using laser-induced breakdown spectroscopy coupled with chelating resin enrichment," *Scientific Reports*, vol. 9, pp. 1–8, 2019.

[192] A. Sarkar, S. K. Aggarwal, K. Sasibhusan, and D. Alamelu, "Determination of sub—ppm levels of boron in ground water samples by laser induced breakdown spectroscopy," *Microchimica Acta*, vol. 168, pp. 65–69, 2010.

[193] F. Zhao, Z. Chen, F. Zhang, R. Li, and J. Zhou, "Ultrasensitive detection of heavy metal ions in tap water by laser-induced breakdown spectroscopy with the assistance of electrical-deposition," *Analytical Methods*, vol. 2, pp. 408–414, 2010.

[194] D. Zhang, A. Chen, Y. Chen et al., "Influence of substrate temperature on the detection sensitivity of surface-enhanced LIBS for analysis of heavy metal elements in water," *Journal of Analytical Atomic Spectrometry*, vol. 36, pp. 1280–1286, 2021.

[195] S. Ma, Y. Tang, S. Zhang et al., "Chlorine and sulfur determination in water using indirect laser-induced breakdown spectroscopy," *Talanta*, vol. 214, Article ID 120849, 2020.

[196] Z. Tang, Z. Hao, R. Zhou et al., "Sensitive analysis of fluorine and chlorine elements in water solution using laser-induced breakdown spectroscopy assisted with molecular synthesis," *Talanta*, vol. 224, Article ID 121784, 2021.

[197] S. Ma, Y. Tang, Y. Ma et al., "The pH effect on the detection of heavy metals in wastewater by laser-induced breakdown spectroscopy coupled with a phase transformation method," *Journal of Analytical Atomic Spectrometry*, vol. 35, pp. 198–203, 2020.

[198] A. F. Y. Haider, B. Rahman, Z. H. Khan, and K. M. Abedin, "Survey of the water bodies for ecotoxic metals by laser-induced breakdown spectroscopy," *Environmental Engineering Science*, vol. 32, pp. 284–291, 2015.

[199] V. Kiris, J. Savovic, A. Nevar et al., "Laser-induced breakdown spectroscopy analysis of water solutions deposited on PTFE surface: influence of copper oxide nanoparticles and NELIBS effect," *Spectrochimica Acta Part B: Atomic Spectroscopy*, vol. 187, Article ID 106333, 2022.

[200] Y. Wang, J. Kang, Y. Chen, and R. Li, "Sensitive analysis of copper in water by LIBS–LIF assisted by simple sample pretreatment," *Journal of Applied Spectroscopy*, vol. 86, pp. 353–359, 2019.

[201] M. S. Cheri and S. Tavassoli, "Quantitative analysis of toxic metals lead and cadmium in water jet by laser-induced breakdown spectroscopy," *Applied Optics*, vol. 50, pp. 1227–1233, 2011.

[202] N. K. Rai, A. K. Rai, A. Kumar, and S. N. Thakur, "Detection sensitivity of laser-induced breakdown spectroscopy for Cr II in liquid samples," *Applied Optics*, vol. 47, pp. G105–G111, 2008.

[203] N. Aras, S. Ü. Yeşiller, D. A. Ateş, and Ş. Yalçın, "Ultrasonic nebulization-sample introduction system for quantitative analysis of liquid samples by laser-induced breakdown spectroscopy," *Spectrochimica Acta Part B: Atomic Spectroscopy*, vol. 74, pp. 87–94, 2012.

[204] H. Sobral, R. Sanginés, and A. Trujillo-Vázquez, "Detection of trace elements in ice and water by laser-induced breakdown spectroscopy," *Spectrochimica Acta Part B: Atomic Spectroscopy*, vol. 78, pp. 62–66, 2012.

[205] M. Wu, X. Wang, G. Niu et al., "Ultrasensitive and simultaneous detection of multielements in aqueous samples based on biomimetic array combined with laser-induced breakdown spectroscopy," *Analytical Chemistry*, vol. 93, 2021.